scientific reports

Check for updates

OPEN

2D and 3D in vitro photodynamic activities of tetra-substituted symmetric water-soluble cationic zinc(II) phthalocyanines on cancer

Seyma Isik[1,2], Mukaddes Ozcesmeci[3], Ayfer Kalkan Burat[3], Esin Hamuryudan[3], Ali Erdogmus[4,5], Ozge Can[6]✉ & Muge Serhatli[2]✉

In this study, the PDT activities of 2,9(10),16(17),23(24)-tetrakis(2-dimethylammoniumethoxy) phthalocyaninatozinc(II) tetraiodide (ZnPc1) and 1,8(11),15(18),22(25)-tetrakis(2-trimethylaminoethoxy)phthalocyaninatozinc(II)tetraiodide (ZnPc2) compounds were investigated in 2D monolayer cultures and 3D spheroids of three human cancer cell lines: human submaxillary salivary gland epidermoid carcinoma (A253), human colon colorectal adenocarcinoma (HT29), and human pharynx squamous carcinoma (FaDu) cells. The results indicate that both molecules are non-toxic in the absence of light, which is a crucial feature of an effective photosensitizer. Upon exposure to light, ZnPc1 exhibited significant cytotoxicity in all three cell lines, particularly in FaDu cells, in both 2D monolayer cultures and 3D spheroids, whereas ZnPc2 showed moderate efficacy compared to ZnPc1. PDT using both phthalocyanine (Pc) molecules resulted in substantial reactive oxygen species (ROS) production. Delayed ROS production is higher than that of immediate ROS, indicating their ability to stimulate ROS production over an extended period and retain an oxidative stress response in the cells rather than immediately after PDT. Among these molecules, ZnPc1 induced both immediate and delayed ROS production more efficiently than ZnPc2. Furthermore, singlet oxygen yields of ZnPc1 were higher than ZnPc2, which is consistent with the cytotoxicity results. These findings confirmed that PDT induces an ROS-mediated cytotoxic response. The mechanisms of cellular death triggered by PDT were evaluated, and the results revealed that apoptosis was the predominant process. These findings underscore the potential of ZnPc1 as a potent photosensitizer in PDT while also highlighting the differences between 2D and 3D culture models in evaluating PDT efficacy. While the 2D system enables simplified cytotoxicity evaluation, the 3D spheroid model better replicates physiologically relevant environment and treatment resistance. This comparison underscores necessity of integrating 3D models in PDT studies for more predictive in vivo insights.

Keywords Cancer, Photodynamic therapy, Phthalocyanine, Reactive oxygen species, Singlet oxygen

Cancer encompasses a group of diseases characterized by the uncontrolled growth of abnormal cells that possess the capability to invade and metastasize to other regions of the body[1]. Various therapeutic modalities are currently approved by the FDA, such as chemotherapy, radiotherapy, immunotherapy, and targeted drug therapy. Among these, photodynamic therapy (PDT) is distinguished by its minimal side effects, selectivity, long-term efficiency, and capacity to circumvent drug resistance[2,3].

PDT is a therapeutic application that combines three essential elements: a light source, non-toxic photosensitizer agent, and molecular oxygen to produce cytotoxic reactive oxygen species (ROS), leading to selective tumor destruction. The first step of this treatment begins with the administration of a tumor-localizing photosensitizer agent, which is subsequently activated by a light source of an appropriate wavelength[4–7]. Upon

[1]Department of Medical Biotechnology, Graduate School of Health Sciences, Acibadem Mehmet Ali Aydinlar University, 34752 Istanbul, Turkey. [2]TUBITAK Marmara Research Center, Climate Change and Life Sciences, Biotechnology Research Group, 41470 Kocaeli, Turkey. [3]Department of Chemistry, Istanbul Technical University, 34469 Istanbul, Turkey. [4]Department of Chemistry, Yildiz Technical University, 34220 Istanbul, Turkey. [5]Health Biotechnology Joint Research and Application Center of Excellence, 34220 Istanbul, Turkey. [6]Department of Biomedical Engineering, Faculty of Engineering and Natural Sciences, Acibadem Mehmet Ali Aydinlar University, 34752 Istanbul, Turkey. ✉email: ozge.can@acibadem.edu.tr; muge.serhatli@tubitak.gov.tr

activation, the photosensitizer transitions from the ground energy state to the triplet energy state, leading to two types of photochemical responses in nearby molecules, predominantly singlet oxygen (excited form of molecular oxygen), in the context of PDT. The photophysical activation of ground state oxygen occurs via two different reactions[8,9]. In type-I reactions, electrons or photons are transferred to molecular oxygen, resulting in the formation of reactive oxygen species. Conversely, in type-II reactions, energy transfer occurs rather than electrons, resulting in generation of singlet oxygen[9,10]. The resulting ROS causes damage and death of cancerous cells. Because this reaction is very short-lived (10–350 ns) and highly localized (approximately 10–55 nm within the cell), the surrounding healthy tissues are not affected[11,12].

PDT-mediated cell death can occur in the form of apoptosis, necrosis, or a combination of both, depending on factors such as light dose, subcellular localization of the photosensitizer, and cell type[5,13]. Typically, lower light doses trigger apoptosis, whereas higher doses cause necrotic cell death owing to the inactivation of apoptosis-related enzymes and components such as caspases[14,15].

Phthalocyanines (Pcs) are synthetic macrocyclic compounds that have garnered significant interest as photosensitizers for PDT applications because of their spectral absorption characteristics and high molecular extinction coefficients in the red Q band[16–18]. Pcs produce 26–30 kcal mole^{-1} of energy in their triplet state, which is appropriate for efficient PDT, as singlet oxygen formation requires 23 kcal mole^{-1}[19,20]. Moreover, Pcs exhibit numerous properties that make them highly valuable in research and clinical settings, including tumor selectivity, non-toxicity, effectiveness as photosensitizers, fluorescence capacities, long-lived triplet state production efficiency upon irradiation, and photochemical and chemical stability[17,21,22]. Pcs can be chemically modified by the addition of functional groups to their peripheral, non-peripheral, or axial locations, thereby improving their water solubility and interaction with target cells, which is important for effective PDT[23–28]. Different metal ions can be introduced into the central ring of metal-free Pcs to modulate their properties. The photoreduction rates of Pcs vary depending on the metal group on the central ring of the metallo Pcs, in the order of Zn > Al > Mg > Sn > Fe[19,29]. Zinc phthalocyanines are distinguished by their high chemical and photochemical stability, high molar extinction coefficient, efficient singlet oxygen generation, low dark toxicity, and excitation at wavelengths greater than 630 nm[16]. The absorption characteristics in the red-light region enable the targeting of tumors located in deeper tissues[30]. Moreover, the cellular uptake of Pcs can be enhanced by the addition of cationic substituents, which provide electrostatic interactions with the negatively charged cell membrane and enable improved phototoxicity through better interactions with cellular components[31]. Various studies have demonstrated the effectiveness of PDT with ZnPc in different cancer cell lines, including human colon carcinoma, human cervical adenocarcinoma, human prostate adenocarcinoma, human breast carcinoma, human lung carcinoma, and human esophageal squamous carcinoma[32–37].

In this study, we report the 2D and 3D in vitro photodynamic therapy activities of peripheral and non-peripheral tetra-substituted cationic zinc phthalocyanines (ZnPc1 and ZnPc2) in three human cancer cell lines: human submaxillary salivary gland epidermoid carcinoma (A253), human colon colorectal adenocarcinoma (HT29), and human pharynx squamous carcinoma (FaDu) cells. PDT-induced cytotoxicity of ZnPcs was determined in both 2D monolayer cultures and 3D spheroids. In addition, PDT-induced ROS production and cellular death mechanisms were evaluated.

Experimental section/methods

Materials

Human submaxillary salivary gland epidermoid carcinoma from 54 years old male (A253, HTB-41), human colon colorectal adenocarcinoma from 44 years old female (HT29, HTB-38, RRID: CVCL 0320), and human pharynx squamous carcinoma from 56 years old male (FaDu, HTB-43) cells were purchased from American Type Culture Collection (ATCC, United States). McCoy's 5A modified medium, Fetal Bovine Serum (FBS), Minimum Essential Medium Eagle with jocklic modification, Dulbecco's phosphate-buffered saline (DPBS), and Hank's Balanced Salt Solution (HBSS) were purchased from Thermo Fisher Scientific (United States). The MycoAlert Plus Mycoplasma Detection Kit was purchased from Lonza (Basel, Switzerland). 2',7' –dichlorofluorescin diacetate (DCFDA), Hoechst 33342 and propidium iodide (PI) were purchased from Sigma Aldrich (United States). The CellTiter-Glo™ 3D Cell Viability Assay was obtained from Promega (United States). The Apoptosis/Necrosis Detection Kit was purchased from Abcam (Cambridge, UK). 1,8-diazabicyclo[5.4.0] undec-7-ene (DBU).

Synthesis and characterization of phthalocyanines

Cationic phthalocyanines **ZnPc1** and **ZnPc2** were synthesized in our laboratory according to previously reported procedures[38,39]. **ZnPc1** and **ZnPc2** were obtained by quaternization of aliphatic nitrogen atoms in ***p-ZnPc*** and ***np-ZnPc*** with methyl iodine. The equipment and synthesis steps were described below.

FTIR spectra were recorded on a Perkin-Elmer Spectrum One FTIR spectrometer, and ^{1}H NMR spectra were recorded on an Agilent 500 MHz spectrometer, using TMS as the internal reference. UV–Vis spectra were recorded using a Scinco LabProPlus UV/Vis spectrophotometer. Mass spectra were obtained using a Bruker Microflex LT MALDI-TOF MS and Agilent 6530 QTOF-LC–MS spectrometers. The spectral data were given in the Supplementary Data file (Figures S1-S18).

General synthetic method of zinc(II) phthalocyanines

Into a screw-capped tube 4-(2-dimethylaminoethoxy)phthalonitrile [0.300 g, 1.394 mmol (for **2a**)] or 3-(2-dimethylaminoethoxy)phthalonitrile [0.300 g, 1.394 mmol (for **3a**)] and anhydrous $Zn(CH_3COO)_2$ (0.064 g, 0.350 mmol) and 2 mL of 2-dimethylaminoethanol were added, then the mixture was stirred at 140 °C for 24 h under nitrogen atmosphere. The reaction mixture was cooled to room temperature and poured into

100 mL ice-cold water. The precipitate was filtered and washed repeatedly with distilled water, methanol, ethanol, and n-hexane.

2,9(10),16(17),23(24)-Tetrakis(2-dimethylaminoethoxy) phthalocyaninatozinc(II) (p-ZnPc)
$C_{48}H_{52}N_{12}O_4Zn$; Yield: 0.126 g (39%). FTIR ν (cm^{-1}): 3051 (Ar–H), 2958–2848 (alkyl-CH), 1606, 1392, 1225, 1044, 744; ^{1}H-NMR (d_6-DMSO, 500 MHz): 9.10 (br, 4H, Ar–H), 8.23 (br, 4H, Ar–H), 7.92 (br, 4H, Ar–H), 5.33 (br, 8H, OCH_2), 4.43 (br, 8H, NCH_2), 3.56 (s, 24H, NCH_3) ppm; UV–Vis (DMF) λ_{max}/nm (Log ε): 352 (4.38), 679 (4.70); MS (MALDI-TOF): *m/z* 926.193 $[M]^+$.

1,8(11),15(18),22(25)-Tetrakis(2-dimethylaminoethoxy) phthalocyaninatozinc(II) (np-ZnPc)
$C_{48}H_{52}N_{12}O_4Zn$; Yield: 0.120 g (37%). FTIR ν (cm^{-1}): 3064 (Ar–H), 2934–2765 (alkyl-CH), 1446, 1236, 1062, 852, 741; ^{1}H-NMR (d_6-DMSO, 500 MHz): 8.92 (br, 4H, Ar–H), 8.07 (br, 4H, Ar–H), 7.69 (br, 4H, Ar–H), 4.76 (br, 8H, OCH_2), 4.57 (br, 8H, NCH_2), 3.41 (s, 24H, NCH_3) ppm; UV–Vis (DMF) λ_{max}/nm (Log ε): 345 (4.21), 697 (4.69); MS (MALDI-TOF): *m/z* 926.413 $[M]^+$.

General synthetic method for cationic zinc phthalocyanines

p-ZnPc [0.120 g; 0.129 mmol (for **ZnPc1**)] or ***np-ZnPc*** [0.120 g; 0.129 mmol (for **ZnPc2**)] was dissolved in 50 mL of chloroform in a single-necked reaction flask. Methyl iodide (0.092 g, 0.648 mmol) was added. The reaction mixture was stirred and refluxed for 20 h. Subsequently, the chloroform was evaporated using a rotary evaporator under vacuum. The resulting solid was washed repeatedly with methanol, ethanol, chloroform, dichloromethane, tetrahydrofuran, and acetone.

2,9(10),16(17),23(24)-Tetrakis(2-dimethylammoniumethoxy)phthalocyaninatozinc(II) tetraiodide (ZnPc1)
$C_{52}H_{64}ZnI_4N_{12}O_4$; Yield: 0.160 g (83%). FTIR ν (cm^{-1}): 3010 (Ar–H), 2949–2826 (alkyl-CH), 1606, 1472, 1225, 1095, 950, 744; ^{1}H-NMR (d_6-DMSO, 500 MHz): 9.38 (br, 4H, Ar–H), 9.05 (br, 4H, Ar–H), 7.91 (br, 4H, Ar–H), 5.12 (br, 8H, OCH_2), 4.13 (br, 8H, NCH_2), 3.42 (s, 36H, NCH_3) ppm; UV–Vis (DMSO) λ_{max}/nm (Log ε): 358 (4.36), 682 (4.70); UV–Vis (H_2O) λ_{max}/nm (Log ε): 340 (4.33), 636 (4.33), 670 (4.11); MS (ESI): *m/z* 748.0326 $[M+2H]^{2+}$.

1,8(11),15(18),22(25)-Tetrakis(2-trimethylaminoethoxy)phthalocyaninatozinc(II) tetraiodide (ZnPc2)
$C_{52}H_{64}ZnI_4N_{12}O_4$; Yield: 0.114 g (59%). FTIR ν (cm^{-1}): 3021 (Ar–H), 2924–2849 (alkyl-CH), 1469, 1235, 853, 742; ^{1}H-NMR (d_6-DMSO, 500 MHz): 9.14 (br, 4H, Ar–H), 8.29 (br, 4H, Ar–H), 7.97 (br, 4H, Ar–H), 5.33 (br, 8H, OCH_2), 4.44 (br, 8H, NCH_2), 3.55 (s, 36H, NCH_3) ppm; UV–Vis (DMSO) λ_{max}/nm (Log ε): 329 (4.15), 704 (4.64); UV–Vis (H_2O) λ_{max}/nm (Log ε): 327 (4.59), 653 (4.27), 694 (4.30). MS (ESI): *m/z* 748.0368 $[M+2H]^{2+}$.

Photochemical studies: singlet oxygen quantum yields (Φ_Δ)

Singlet oxygen quantum yield (Φ_Δ) was analyzed by using the interested method with ZnPc in DMSO or $ZnPcS_{mix}$ in aqueous media as standard. DPBF and ADMA were used as chemical quenchers for singlet oxygen determination in DMSO and aqueous media, respectively. Equation (1) was used for the calculations:

$$\Phi_\Delta = \Phi_\Delta^{std} \frac{R.I_{abs}^{std}}{R^{std}.I_{abs}} \quad (1)$$

where Φ_Δ^{std} is the singlet oxygen quantum yield for the standards unsubstituted ZnPc $\left(\Phi_\Delta^{std} = 0.67 \text{ in DMSO}\right)$ or $ZnPcS_{mix}$ $\left(\Phi_\Delta^{std} = 0.45 \text{ in aqueous media}\right)$. R and R_{Std} are the DPBF (or ADMA) photobleaching rates in the presence of the respective samples (**ZnPc1** and **ZnPc2**) and standards, respectively. I_{abs} and I_{abs}^{std} are the rates of light absorption by the samples (**ZnPc1** and **ZnPc2**) and standards, respectively. The sensitizer solutions that contain DPBF (or ADMA) were prepared in the dark and irradiated in the Q band region using the set-up described above. DPBF degradation at 417 nm and ADMA degradation at 380 nm were observed[40].

In vitro studies

Cell culture
A253 and HT29 cells were cultured in McCoy's 5A modified medium supplemented with fetal bovine serum (FBS, 10%, v/v) and penicillin–streptomycin (1%, v/v). FaDu cells were cultured in Minimum Essential Medium Eagle with jocklic modification, supplemented with FBS (10%, v/v) and penicillin–streptomycin (1%, v/v). Mycoplasma tests were conducted monthly on the cell lines using a Lucetta 2 Luminometer and a MycoAlert Plus Mycoplasma Detection Kit.

Dark cytotoxicity
The cells were seeded in 96 well plates (5×10^3 cells/well) and cultured for 24 h in a humidified incubator (37 °C, 5% CO_2). After incubation, varying concentrations of Pc (1, 10 and 100 μM) were administered to the cells and shielded from light. After 24 h, cell viability was determined using the WST-1 assay. The concentration range of Pc molecules for photodynamic therapy was determined based on dark cytotoxicity data to ensure appropriate dosing for effective treatment. All analyses were performed blinded, and data analysis were unaware of the treatments.

Photodynamic therapy
Cells were seeded into 96-well plates at a density of 5×10^3 cells/well and incubated for 24 h in a humidified incubator (37 °C, 5% CO_2). Pc molecules were then administered at concentrations of 1 µM and 10 µM for endpoint analyses and 100 pM, 1 nM, 10 nM, 100 nM, 1 µM, 10 µM, and 100 µM for real-time assays, followed by a 1 h incubation to facilitate cellular uptake. After incubation, the Pc-containing medium was replaced with fresh culture medium to remove residual extracellular molecules. PDT was performed using the ceLED system (CETONI, Germany) at 650–670 nm, with a fluence rate of 75 mW cm-2 and a light dose of 20 J cm-2 (exposure time: 270 s)[41]. The temperature was strictly maintained at 37 °C throughout irradiation. Following PDT, cells were incubated under dark conditions (37 °C, 5% CO_2) to prevent unintended phototoxicity.

Reactive oxygen species (ROS) production
PDT-induced ROS production on the cells were determined using 2′, 7′-dichlorofluorescin diacetate (DCFDA)[42]. The cells were seeded in the wells of 96-well plate (5×10^3 cells/well) and incubated for 24 h (37 °C, 5% CO_2). Then, Pc molecules (1 and 10 µM) were administered to the cells, PDT (20 J cm^{-2}, 650–670 nm) was applied, and incubated for 30 min (immediate ROS production) and 24 h (late ROS production) in a humidified incubator (37 °C, 5% CO_2). Following the incubation, the cells were treated with DCFDA (20 µM in HBSS), incubated for 30 min at 37 °C. The endpoint fluorescence intensities (λ_ex = 504 nm, λ_em = 529 nm) were measured using Cytation 5 (Agilent, United States).

PDT-induced cytotoxicity
The cells were seeded in the wells of 96-well plate (5×10^3 cells/well) and incubated for 24 h (37 °C, 5% CO_2). Then, Pc molecules (1 and 10 µM) were administered to the cells, PDT (20 J cm^{-2}, 650–670 nm) was applied. 24 h post-PDT, phototoxicity was determined using WST-1 assay. Briefly, medium was replaced by WST-1 solution (1:10 in complete medium), incubated at 37 °C for 3 h, and absorbance was measured at 450/600 nm. Cell viability were normalized to untreated control.

Real-time proliferation inhibition
Real-time proliferation inhibition of Pc-mediated PDT on cancer cells was analyzed using the impedance-based xCELLigence MP system (Agilent Technologies, United States). The cells were suspended in complete medium, seeded onto a 16-well E-plate of the xCELLigence real time cell analyzer (RTCA) MP, then incubated for 24 h (37 °C, 5% CO_2). Next, Pc molecules (100 pM-100 µM) were administered to the cells, PDT (20 J cm^{-2}, 650–670 nm) was applied, and incubated in the device (37 °C, 5% CO_2). Real-time data for each cell line were collected for 200 h at 15 min intervals, and the half-maximal inhibitory concentrations (IC_{50}) of Pc molecules were determined from the graph of cell index versus log concentration of Pcs. The real time data were given in the Supplementary Data file (Figures S19-S24).

PDT-induced cytotoxicity on 3D cancer spheroids
The cellular response of cancer spheroids to PDT was determined using fluorescence staining (Live/Dead) and a luminescence-based assay. The 3D cancer spheroids were formed on a 96-well Ultra-Low Attachment Spheroid Microplate (Corning, United States). Then, Pc molecules (10 µM) were administered to the spheroids, PDT (20 J cm^{-2}, 650–670 nm) was applied, and incubated for 72 h in a humidified incubator (37 °C, 5% CO_2). For image-based live/dead analysis, the cells were stained with Hoechst 33,342 (2 µg mL^{-1} in HBSS) and propidium iodide (PI, 8 µg mL^{-1} in HBSS), incubated for 60 min, and images were taken using Cytation 5 (Agilent, United States). In addition, a quantitative analysis of PDT-induced cytotoxicity in cancer spheroids was conducted using a luminescence-based assay (CellTiter-Glo ™ 3D Cell Viability Assay, Promega) according to the manufacturer's instructions. Briefly, 100 µL of the assay solution was added to the spheroids, and the spheroids were incubated for 25 min. Afterwards, luminescence was measured using Cytation 5 (Agilent, United States), and the data were normalized to the untreated control.

Cellular death mechanism
PDT-induced cellular death mechanisms were determined using the Apoptosis/Necrosis Detection Kit (Abcam, Ab176749), according to the manufacturer's instructions. The cells were seeded in the wells of 96-ell plate (10^4 cells/well) and incubated for 24 h (37 °C, 5% CO_2). Afterwards, Pc molecules (1–10 µM) were administered to the cells, PDT (20 J cm^{-2}, 650–670 nm) was applied, and incubated for 24 h in a humidified incubator (37 °C, 5% CO_2). The cells were then stained with CytoCalcein Violet 450, Apopxin Green, and 7-ADD, incubated for 60 min, and images were taken using Cytation 5 (Agilent, United States). The number of apoptotic and necrotic cells was counted from the captured images using Gen5 software (Agilent, United States).

Statistics
Data are expressed as the mean ± SD. Comparisons between groups were performed using a two-way ANOVA with post hoc test. GraphPad Prism (RRID:SCR_002798) was used for statistical analysis. Statistical significance was set at $p < 0.05$.

Results
The in vitro PDT activities of peripheral and non-peripheral cationic zinc phthalocyanines (ZnPc1 and ZnPc2) was investigated in A253, HT29, and FaDu cancer cell lines, focusing on cytotoxicity in 2D monolayers and 3D spheroids, as well as ROS generation and cell death mechanism (Fig. 1).

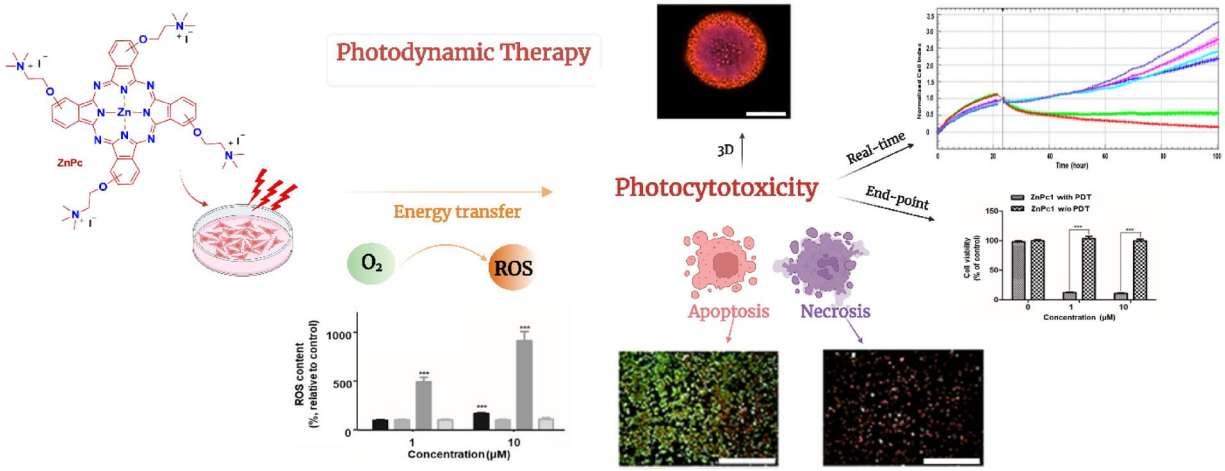

Fig. 1. Schematic representation of ZnPc-mediated PDT, which illustrates the activation of ZnPc by light, leading to the production of reactive oxygen species (ROS) through energy transfer. These ROS induce cellular damage, resulting in apoptosis and necrosis, as demonstrated by real-time monitoring and endpoint analyses.

Characterization of Pc molecules

Phthalocyanines were synthesized and characterized using FT-IR, ^{1}H NMR, and UV-Vis spectroscopic techniques. The spectral data (Figures S1-S18) for each compound matched the formula (Figure 2). The FT-IR spectra of cationic phthalocyanines (ZnPc1 and ZnPc2) showed aromatic CH, aliphatic CH, and ether (C–O–C) stretching vibrations at 3010–3021, 2924–2849, and 1225–1235 cm^{-1}, respectively (Figures S11 and S12). The ^{1}H NMR spectra of ZnPc1 and ZnPc2, aromatic protons were observed in the range of 9.38–7.91 ppm (for ZnPc1) and 9.14–7.97 ppm (for ZnPc2), OCH_2 protons were observed at 5.12 ppm (for ZnPc1) and 5.33 ppm (for ZnPc2), NCH_2 protons were observed at 4.13 ppm (for ZnPc1) and 4.44 ppm (for ZnPc2), and NCH_3 protons were observed as singlets at 3.42 ppm (for ZnPc1) and 3.55 ppm (for ZnPc2) (Figures S3 and S4). UV-Vis spectroscopy was employed to analyze the electronic spectra of phthalocyanine molecules (ZnPc1 and ZnPc2) in dimethyl sulfoxide (DMSO) and aqueous solutions (water). In DMSO, the cationic zinc phthalocyanines ZnPc1 and ZnPc2 exhibited distinct single narrow Q-bands at 682 and 704 nm, respectively, while in water, they produced doublet Q bands at 636 and 670 nm (for ZnPc1) and 653 and 694 nm (for ZnPc2), respectively (Figures S15–S18). The intensities of the Q-bands were notably higher in DMSO than in water. Furthermore, ZnPc1 demonstrated a higher Q-band intensity than ZnPc2, indicating a more pronounced electronic transition. Additionally, B-bands were observed at approximately 340 nm for ZnPc1 and 327 nm for ZnPc2. The mass spectra showed the molecular ion peaks at $m/z = 748.0326$ $[M+2H]^{2+}$ for ZnPc1 and 748.0368 $[M+2H]^{2+}$ for ZnPc2 (Figures S7 and S8).

In singlet oxygen quantum yield (Φ_Δ) measurements carried out in a dark room, solutions containing 1,3-diphenylisobenzofuran (DPBF), which is used as chemical quencher and **ZnPc1** and **ZnPc2** were exposed to light (intensity of 7.05×10^{15} photons s^{-1} cm^{-2}) every 5 s and the changes in absorption of DPBF at 417 nm in DMSO and ADMA at 380 nm in aqua solution were observed. Related spectra and plots of the decrease in absorbance of DPBF against time were shown in Fig. 3A,B (in DMSO) and Fig. 3C,D (in H_2O).

Singlet oxygen quantum yield (Φ_Δ) value was listed in Table 1. The obtained spectra and time-dependent decrease of absorbance at 417 nm of DPBF and 380 nm of ADMA were shown in Fig. 3. In the calculations using DBPF and ADMA as standards, the singlet oxygen quantum yields of **ZnPc1** and **ZnPc2** were calculated as 0.79 (Fig. 3A) and 0.60 (Fig. 3B) in DMSO, 0.47 (Fig. 3C) and 0.37 (Fig. 3D) in aqua solution, respectively. No change was observed in the absorption band intensities of Pc compounds during singlet oxygen measurements.

PDT-induced ROS production

To investigate cellular damage, PDT-induced cellular ROS levels were determined using DCFDA. To elucidate this mechanism, ROS formation was detected at two specific time points: 30 min (immediate) and 24 h (delayed) post-PDT. These results demonstrated that ZnPc1-mediated PDT induced immediate ROS production across each cell line to varying degrees. FaDu cells (Fig. 4A) exhibited the highest ROS levels, followed by HT29 (Fig. 4C) and A253 (Fig. 4B) cells. ZnPc2-mediated PDT induced moderate immediate ROS production in FaDu (Fig. 4D) and HT29 (Fig. 4F) cells, but only at high doses, where there was no significant difference was observed in A253 cells (Fig. 4E). Similar to immediate ROS production, PDT with both ZnPc1 and ZnPc2 molecules resulted in the highest level of delayed ROS production in FaDu cells, followed by HT29 and A253 cells. Additionally, PDT with ZnPc1 caused significantly higher ROS levels in each cell line compared to ZnPc2.

PDT-induced cellular response on 2D monolayer cultures and 3D spheroids

The colorimetric WST-1 assay was used to evaluate the dark- and PDT-induced cytotoxicity of ZnPc1 and ZnPc2 on A253, FaDu, and HT29 cells. The results demonstrated that both ZnPc1 and ZnPc2 at concentrations up to 10 μM exhibited no significant cytotoxicity in the absence of light across all three cell lines. FaDu cells

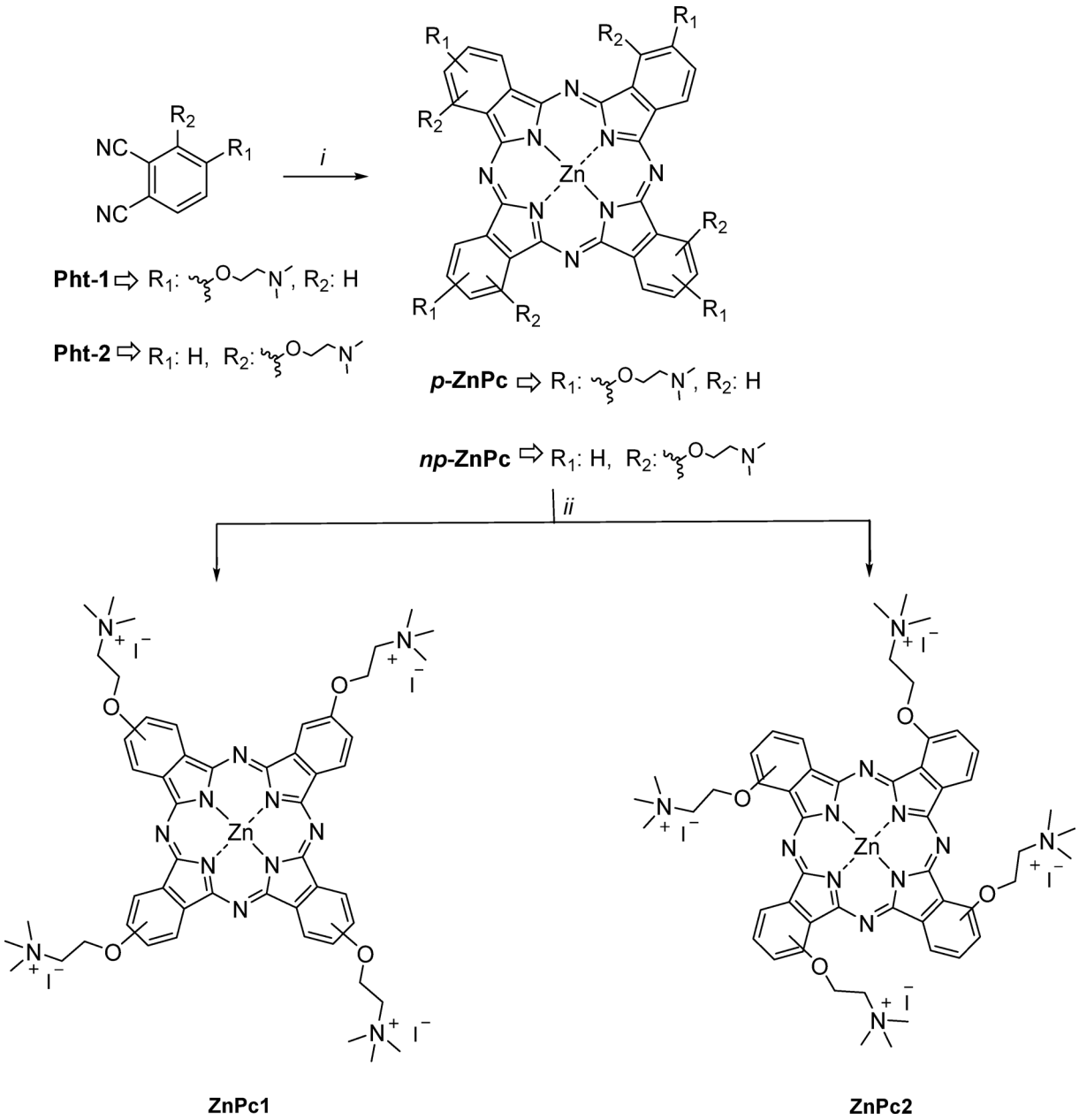

Fig. 2. Synthetic route to peripheral (ZnPc1) and non-peripheral (ZnPc2) tetra-substituted cationic zinc phthalocyanines (*i*. $Zn(CH_3COO)_2$, 2-dimethylaminoethanol, 140 °C, 24 h. *ii*. CH_3I, $CHCl_3$, at dark, reflux temperature, 20 h).

(Fig. 5A) exhibited the highest PDT-induced cytotoxicity, with both high and low doses of ZnPc1 resulting in approximately 90% cell death compared with the untreated control. Similarly, PDT with a high dose of ZnPc2 also induced significant cell death in FaDu cells, whereas a low dose of ZnPc2 caused minimal cytotoxicity (Fig. 5D). A253 (Fig. 5B) and HT29 (Fig. 5C) cells showed a significant response to PDT at both high and low doses of ZnPc1. In contrast, a high dose of ZnPc2 induced moderate cell death in both A253 and HT29 cells, whereas a low dose of ZnPc2 had negligible effects on cell viability (Fig. 5D–F).

The effect of Pc-mediated PDT on cancer cell proliferation was evaluated using a real-time cell analysis (RTCA) system. The principle of the equipment involves the conversion of electrical current into a unitless cell index (CI), which was measured at 15 min intervals. An increase in CI indicates cell proliferation, whereas a decrease indicates cell death. The half-maximal inhibitory concentration (IC_{50}) values of Pc molecules (with PDT) were calculated from the sigmoidal dose–response curve (DRC) generated over normalized CI values (between 24 and 96 h, post-treatment) using RTCA-Software. The concentration range of Pc molecules, 100 pM to 100 µM, was studied in all cell lines (Figures S19-S24). The IC_{50} values for ZnPc1 were 0.275, 1.447, and 0.413 µM for FaDu (Figure S19), A253 (Figure S20), and HT29 (Figure S21) cells, respectively. In contrast, the IC_{50} values for ZnPc2 were 1.544, 8.485, and 4.654 µM for FaDu (Figure S22), A253 (Figure S23), and

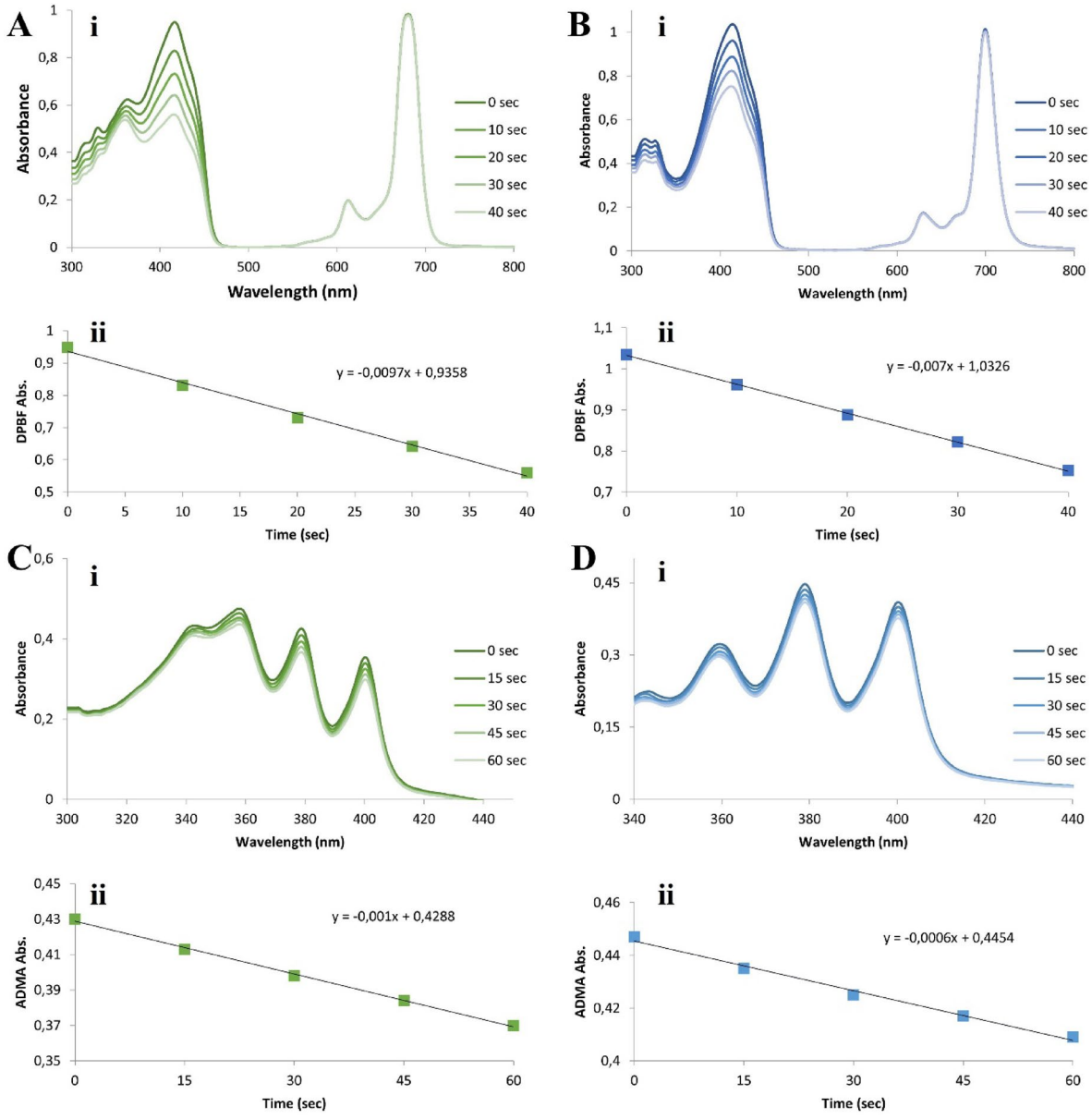

Fig. 3. Change in UV–Vis spectrum of singlet oxygen measurement of complex (**A**) ZnPc1 and (**B**) ZnPc2 in DMSO by photochemical study (observed peak: 414 nm and 416 nm), (**C**) ZnPc1 and (**D**) ZnPc2 in water by photochemical study (observed peak: 379 nm for both). (i) UV–Vis spectrum, and (ii) plots of the decrease in absorbance of DPBF or ADMA against time.

Complex	Solvent	$\Phi_{\Delta PDT}$
ZnPc 1	DMSO	0.79
	Water	0.47
ZnPc 2	DMSO	0.60
	Water	0.37

Table 1. Photochemical properties of ZnPc1 and ZnPc2.

HT29 (Figure S24) cells, respectively. The lower IC_{50} values observed for the ZnPc1 molecule across all cell lines indicated its higher potency compared to the ZnPc2 molecule. FaDU cells exhibited the highest sensitivity to ZnPc1-mediated PDT, with an IC_{50} value of 0.275 μM, indicating strong potential for head and neck squamous cell carcinoma. Furthermore, the moderate IC_{50} values for A253 and HT29 cells also indicate the effectiveness of ZnPc1 against salivary gland and colorectal carcinomas. On the other hand, the higher IC_{50} values for the

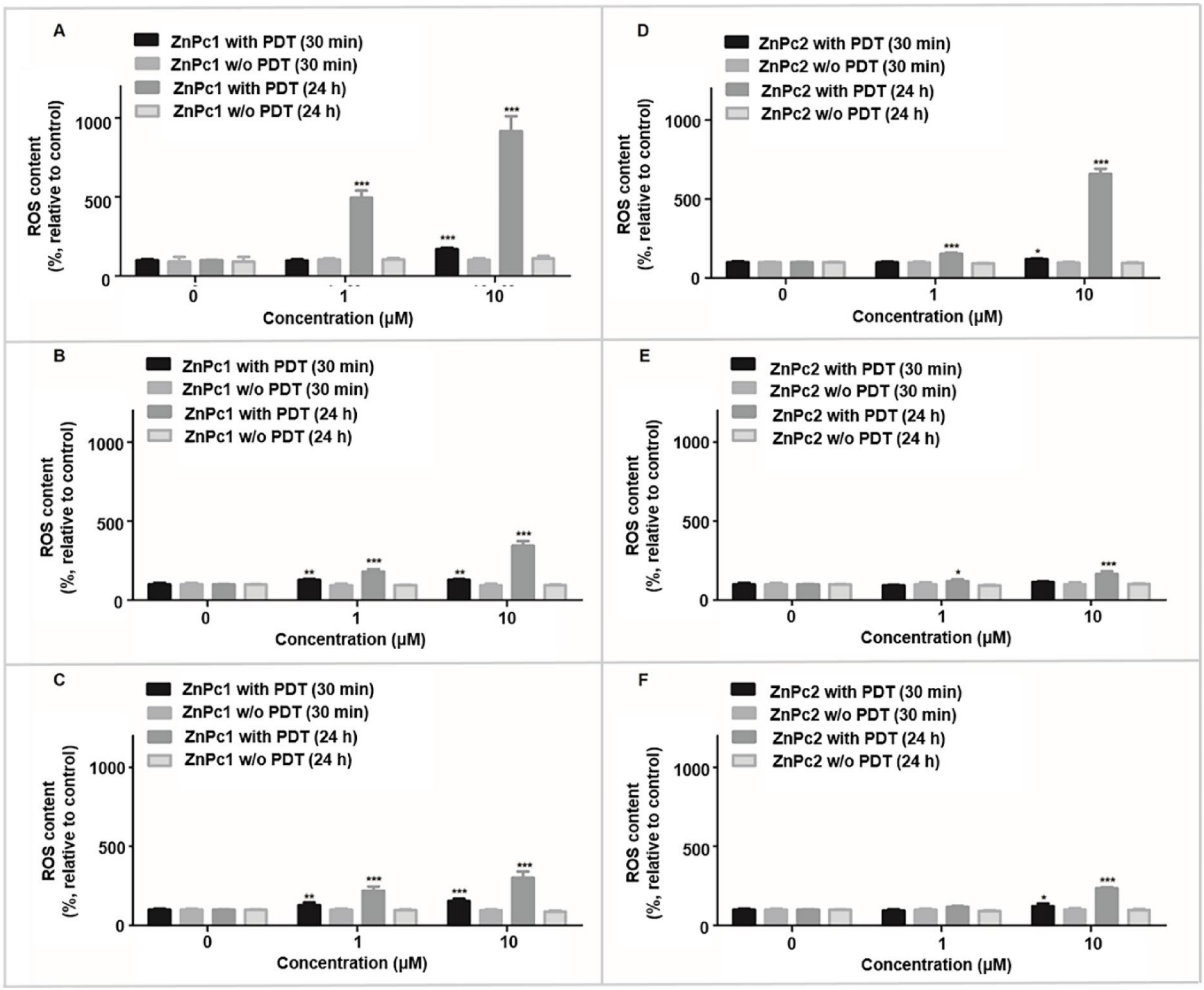

Fig. 4. PDT-induced ROS production in (**A**, **D**) FaDu, (**B**, **E**) A253, and (**C**, **F**) HT29 cells. Results are means ± SD of three independent experiments. $^{*}p < 0.05$, $^{**}p < 0.01$ and $^{***}p < 0.001$. PDT light dose: 20 J cm^{-2}.

ZnPc2 molecule indicated a lower potency of the molecule compared to ZnPc1. A253 cells, with an IC_{50} value of 8.485 μM, showed the least sensitivity to ZnPc2-mediated PDT. The R2 values represent the coefficient of determination, indicating how well the regression model explains the variance in the experimental data. With all R2 values exceeding 0.95, the model provides a highly accurate representation of the IC_{50} values for ZnPc1 and ZnPc2 across the tested cell lines, ensuring the reliability of the results.

In addition to the 2D monolayer culture, the response of cancer cells to PDT was assessed using 3D spheroids. The results indicated that the Pc molecules were non-toxic in the dark and appropriate for PDT applications, as both ZnPc1 and ZnPc2 molecules did not elicit cytotoxic responses in cancer spheroids in the absence of light (Figs. 6, 7, 8). Upon light activation, PDT with both molecules induced significant cytotoxicity in FaDu spheroids (Fig. 6). In contrast, the A253 (Fig. 7) and HT29 (Fig. 8) spheroids exhibited relatively lower cytotoxic responses, indicating that the efficacy of PDT with these Pc molecules varies depending on the cancer cell type. The quantitative assay confirmed the findings of the live/dead assay, indicating reliability of the results.

Cellular death mechanism (apoptosis/necrosis)

The cellular death mechanism induced by Pc-mediated PDT in the cancer cell lines was studied by fluorescence staining with Apoxin Green, Cyto Calcein Violet 450, and 7-AAD. One of the initial events in apoptosis is the translocation of phosphatidylserine (PS) from the inner to the outer surface of the plasma membrane[43]. Apopxin Green binds these negatively charged phosphatidylserine units, enabling the identification of apoptotic cells (green), whereas CytoCalcein Violet 450 stains live (blue) and 7-AAD necrotic (red) cells. Following 24 h of PDT, live cell images were obtained using fluorescence microscopy, and the number of apoptotic and necrotic cells was counted from the captured images. The results demonstrated that PDT with a low dose of both molecules predominantly triggered apoptosis in FaDu (Fig. 9) and A253 (Fig. 10) cells with lower levels of necrosis. However, a dose-dependent increase was observed at higher doses. In contrast, at each dose, HT29 cells (Fig. 11) primarily exhibited necrotic cell death, with only a small fraction of apoptotic cells.

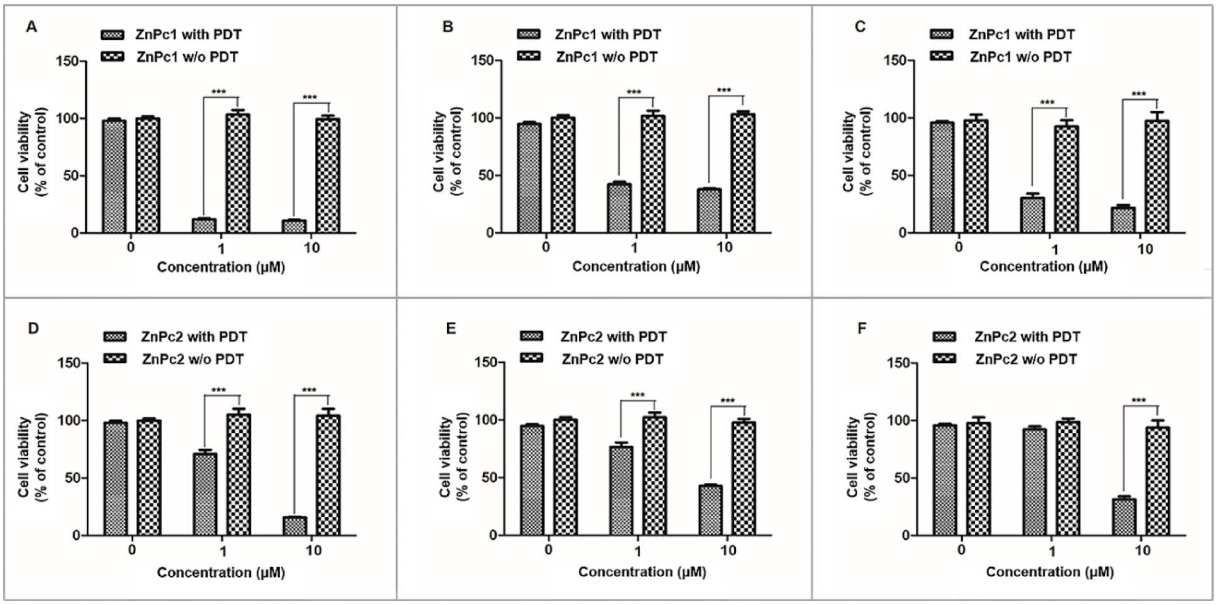

Fig. 5. Dark and PDT-induced cytotoxicity of ZnPcs. PDT with the ZnPc1 molecule induced a dose-dependent cytotoxicity, without affecting cell viability in the absence of light on (**A**) FaDu, (**B**) A253, (**C**) HT29 cell. In contrast, PDT with the ZnPc2 molecule caused significant cytotoxicity only at high doses, without affecting cell viability in the absence of light on (**D**) FaDu cells, (**E**) A253 cells, (**F**) HT29 cells. Results are shown as means ± SD of three independent experiments. $^{*}p < 0.05$, $^{**}p < 0.01$ and $^{***}p < 0.001$.

Discussion

This study investigated the photophysical properties and therapeutic potential of two zinc phthalocyanine derivatives, ZnPc1 and ZnPc2, for PDT applications. The analysis encompassed both immediate and sustained ROS generation, along with evaluation of their impact on cellular viability and death mechanisms. A comparative assessment revealed distinct differences between ZnPc1 and ZnPc2 in terms of phototoxic efficiency and ROS production, offering critical insights into their relative suitability as photosensitizers in PDT. The findings also revealed that the solvent environment significantly influenced the electronic properties of these compounds, affecting their ability to produce ROS and induce cytotoxicity in cells. This solvent sensitivity suggests that optimizing the solvent conditions could enhance the photophysical properties of ZnPc1 and ZnPc2, thereby improving their effectiveness in PDT applications.

Low cytotoxicity in the absence of light is an essential characteristic of effective photosensitizers for PDT applications. The endpoint cytotoxicity results showed that the studied molecules were non-toxic in the dark, thus meeting the fundamental requirement for an effective photosentisizer. Upon photoactivation during PDT, both ZnPc1 and ZnPc2 elicit significant cytotoxic effects, with ZnPc1 showing a particularly pronounced ability to induce cell death. In addition to the endpoint cytotoxicity assay, an impedance-based real-time proliferation inhibition assay was performed to evaluate cellular responses to PDT with ZnPc1 and ZnPc2. Real-time assays, by monitoring dynamic cellular behavior, provide a more accurate and realistic assessment of primary responses than endpoint measurements, and the real-time proliferation inhibition data aligned with the endpoint cytotoxicity findings further supported the observed potency differences between ZnPc1 and ZnPc2 and confirmed their differential efficacy as photosensitizers in PDT. The pronounced cytotoxicity observed across all cell lines, particularly in FaDU cells, with both high and low doses of ZnPc1 highlights its potential as a highly effective photosensitizer. In contrast, the minimal cytotoxicity observed, especially at low doses of ZnPc2, suggests limited therapeutic efficacy. The difference in the PDT activity between ZnPc1 and ZnPc2 indicated the effect of the chemical structure of the photosensitizer on the cellular response. The nature of peripheral substituents can considerably influence the PDT activity of ZnPc. Although the central metal ion and core structure remain unchanged, modifications of the periphery can have a significant impact on the physicochemical properties and biological interactions of the photosensitizer. The absorption and emission spectra of ZnPcs can be shifted by peripheral substituents, thereby optimizing their use in the therapeutic window (650–800 nm) where tissue penetration is maximized. This spectral tailoring has the potential to improve the efficiency of light absorption and ROS generation[44]. Effective PDT depends on the quantum yield of singlet oxygen generation, which is influenced by the presence of electron-donating or electron-withdrawing groups. This can affect the intersystem crossing efficacy in the triplet state[38]. The lifetime of ZnPcs is extended, and the probability of ROS generation increases upon light activation because of the stabilization of the triplet state by peripheral groups. Additionally, substituents that inhibit aggregation can preserve the photophysical properties crucial for the efficient production of ROS[39]. Marino et al. (2010) reported that although both ZnPc1 and ZnPc2 molecules exhibit Q-bands at similar wavelengths, the fluorescence quantum yield (FF) and singlet oxygen quantum yield (FD) values of ZnPc1 molecules are slightly higher than those of ZnPc2, particularly in

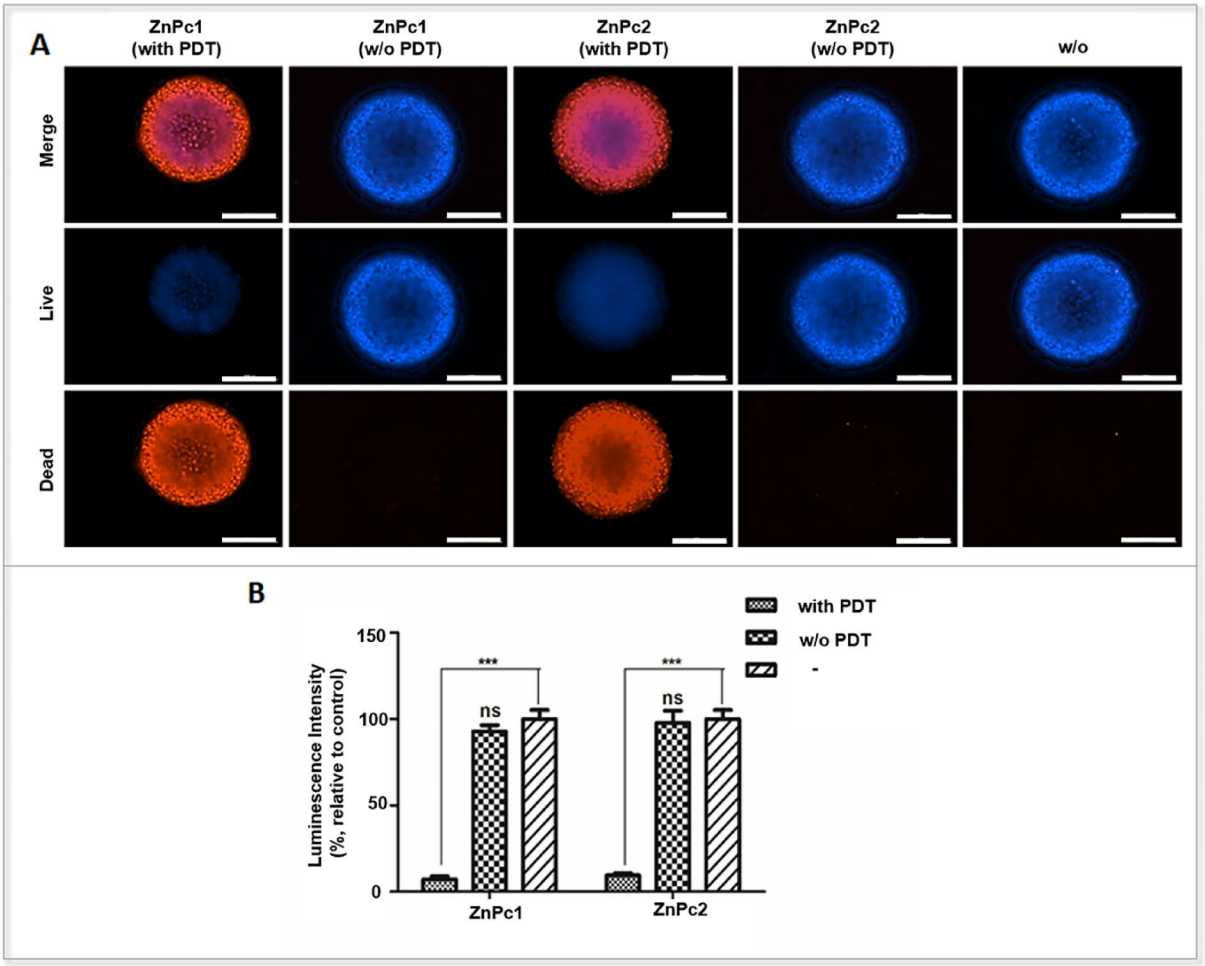

Fig. 6. Pc-mediated PDT on FaDu spheroids. (**A**) Live/dead staining, living cells (Hoechts 3342, blue), dead cells (PI, red), (**B**) ATP-based luminescence cytotoxicity assay. Results are means ± SD of six replicates. $^{*}p < 0.05$, $^{**}p < 0.01$ and $^{***}p < 0.001$. Scale bar: 200 µm.

water. Moreoever, ZnPc1 showed higher photostability with a lower photodegradation constant *k*, indicating its enhanced efficacy in PDT through sustained singlet oxygen production[45]. On the other hand, FaDu cells exhibited the highest cellular response to both molecules, followed by HT29 and A253 cells, indicating the variation in cellular response to PDT among different cell types. Wöhrle et al. (1990), studied the efffect of PDT with ZnPc, which has particularly the same chemical structure with the ZnPc1 molecule, and reported its substantial PDT activity with varying efficacy among different cell lines[46]. In contrast, Marino, et. al. (2010) studied PDT with ZnPcs, ZnPc1 and ZnPc2, and revealed that those molecules, with concentration up to 10 µM, did not lead to sufficient cytotoxicity on Human Nasopharynx Carcinoma (KB Cells)[45]. The different cellular response to Pc-mediated PDT reported in various studies highlighted that the efficacy of Pc is highly dependent on the cell type.

The variations observed in PDT-induced cytotoxicity between ZnPc1 and ZnPc2 across different cell lines can be attributed to a combination of structural differences, photophysical properties, ROS generation efficiency, and cell line-specific factors. ZnPc1, with its peripheral substitution, exhibits superior photophysical characteristics, including higher Q-band intensity, greater photostability, and a more efficient singlet oxygen quantum yield. UV–Vis spectral analysis further confirms that ZnPc1 has a higher Q-band intensity and improved photostability compared to ZnPc2. This suggests that ZnPc1 has a greater ability to absorb and utilize light energy for ROS production, thereby enhancing its photodynamic efficacy. Since PDT efficacy is primarily driven by ROS-mediated cytotoxicity, these differences in ROS generation directly correlate with the superior photodynamic effects of ZnPc1.

The efficacy of PDT is influenced by several critical factors, including the type of photosensitizer used, its concentration, intracellular localization, as well as the light dose and exposure duration. Among these, the most significant determinant of PDT effectiveness is the local oxygen concentration around the photosensitizer[47]. In the absence of sufficient oxygen, the excited-state energy of the photosensitizer is dissipated through non-radiative decay pathways, limiting therapeutic outcomes. In Type II photochemical reactions, the photosensitizer transfers its excited energy directly to molecular oxygen (triplet oxygen), the most stable and prevalent form

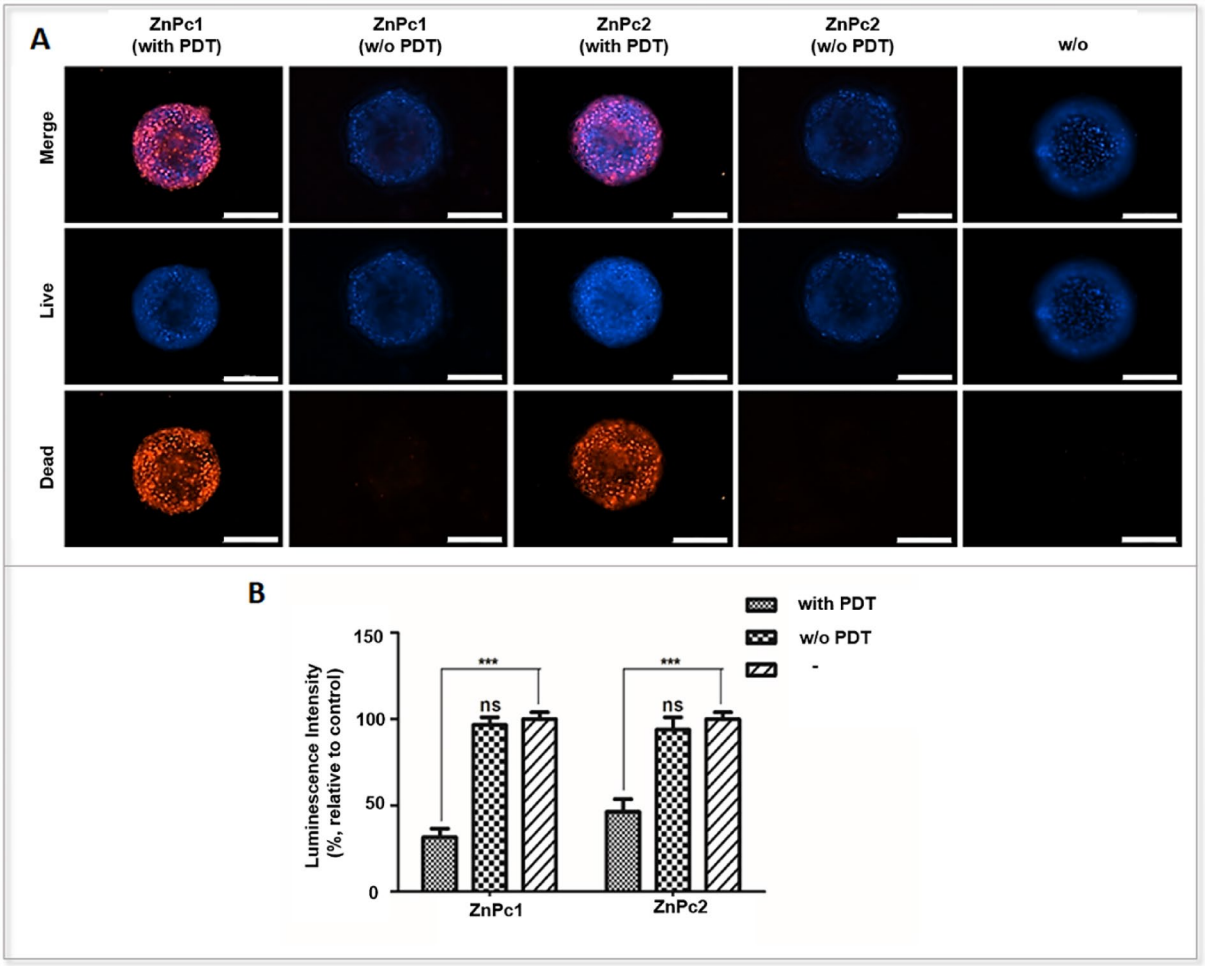

Fig. 7. Pc-mediated PDT on A253 spheroids. (**A**) Live/dead staining, living cells (Hoechts 3342, blue), dead cells (PI, red), (**B**) ATP-based luminescence cytotoxicity assay. Results are means ± SD of six replicates. $^{*}p < 0.05$, $^{**}p < 0.01$ and $^{***}p < 0.001$. Scale bar: 200 µm.

of oxygen in biological systems, generating highly cytotoxic reactive oxygen species such as singlet oxygen. Therefore, the selection of an appropriate photosensitizer is a pivotal step in PDT, as it directly governs the generation of singlet oxygen and, consequently, the therapeutic efficacy of the treatment[48]. Phthalocyanine compounds hold a prominent position among second- and third-generation photosensitizers used in PDT. Due to their strong light absorption in the visible and near-infrared regions, they enable deeper tissue penetration, which is crucial for effective treatment of solid tumors[49]. Their high photochemical stability and long excited-state lifetimes enhance the efficiency of singlet oxygen generation, thereby improving the overall efficacy of PDT[50]. Moreover, the chemical structure of phthalocyanines can be easily modified, allowing functionalization with hydrophilic or lipophilic groups to improve cellular targeting and bioavailability[51]. These features make phthalocyanine derivatives promising candidates for selective delivery to cancer cells while minimizing damage to healthy tissues, ultimately providing a safer and more effective therapeutic approach. The primary mechanism of PDT relies on the generation of reactive oxygen species, particularly singlet oxygen ($^1O_2$), following the activation of a photosensitizer by light. Therefore, quantitative measurement of singlet oxygen production is a critical step in evaluating the photodynamic efficiency of a given photosensitizer. Pre-treatment assessment of singlet oxygen generation allows for the optimization of treatment parameters by indicating the extent to which the photosensitizer can become active in the presence of oxygen[52]. Furthermore, such measurements are essential for determining appropriate dosages and minimizing the risk of phototoxic side effects. The singlet oxygen quantum yields ($\Phi\Delta$) of the studied zinc phthalocyanine derivatives reveal a clear difference in photodynamic efficiency. ZnPc1, which carries peripheral substituents, exhibited a quantum yield of 0.79, whereas the non-peripherally substituted ZnPc2 showed a lower value of 0.60 in DMSO. This disparity suggests that the substitution pattern on the phthalocyanine macrocycle significantly affects its photophysical properties. Peripheral substitution likely enhances intersystem crossing and facilitates more effective interaction with molecular oxygen, resulting in higher singlet oxygen generation[53]. Consequently, ZnPc1 demonstrates greater potential for applications such as photodynamic therapy, where efficient singlet oxygen production is crucial. However, when measured in aqueous solution, both compounds showed lower quantum yields: 0.47 for ZnPc1

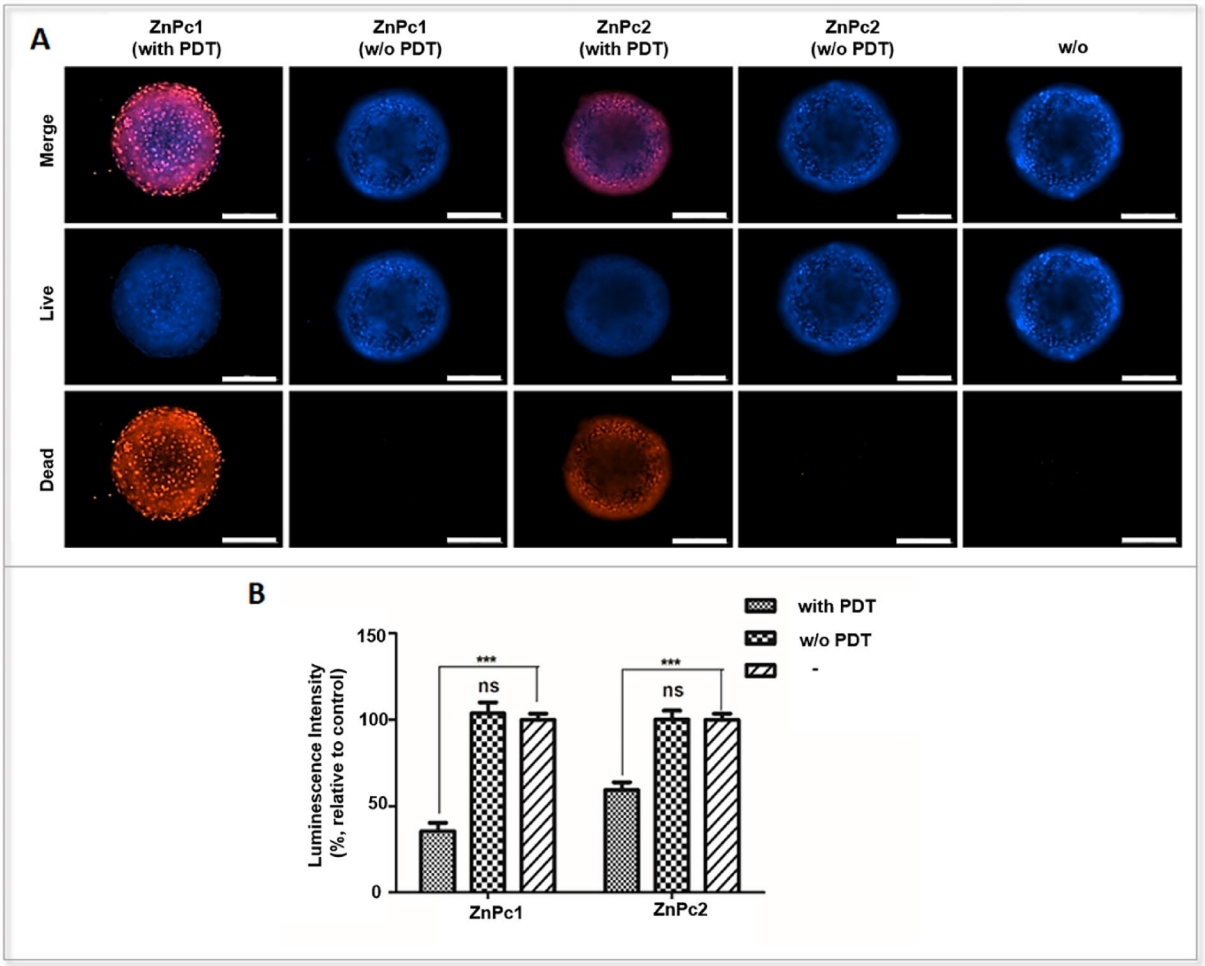

Fig. 8. Pc-mediated PDT on HT29 spheroids. (**A**) Live/dead staining, living cells (Hoechts 3342, blue), dead cells (PI, red), (**B**) ATP-based luminescence cytotoxicity assay. Results are means ± SD of six replicates. $^{*}p < 0.05$, $^{**}p < 0.01$ and $^{***}p < 0.001$. Scale bar: 200 µm.

and 0.39 for ZnPc2. The decrease in singlet oxygen generation in water can be attributed to several factors, including aggregation tendencies of phthalocyanines in polar solvents, reduced solubility, and quenching effects by water molecules[54]. These effects can hinder the excited-state dynamics and the interaction between the triplet state of the photosensitizer and molecular oxygen. Despite the overall reduction in efficiency in water, ZnPc1 still maintains a relatively higher singlet oxygen yield than ZnPc2, reinforcing the beneficial role of peripheral substitution even in biologically relevant environments. Singlet oxygen quantum yield measurements could not be performed in the biological solvent system due to the absence of a suitable reference standard. Accurate determination of quantum yields requires a well-characterized standard with known singlet oxygen efficiency under identical experimental conditions. However, in biologically relevant media, the lack of such a standard, compatible in terms of solubility, photostability, and spectral overlap, precluded reliable comparative measurements. As a result, ΦΔ values could only be obtained in organic and aqueous media, where appropriate standards were available.

Beyond photophysical differences, cell line-dependent variations in photosensitizer uptake and response to oxidative stress also play a crucial role. FaDu cells exhibited the highest sensitivity to ZnPc1, as indicated by the lowest IC50 values, suggesting enhanced cellular uptake and efficient ROS-induced phototoxicity. In contrast, A253 and HT29 cells displayed moderate responses, likely due to differences in antioxidant defenses, membrane permeability, and ROS detoxification mechanisms, which influence their susceptibility to PDT-induced oxidative stress.

Taken together, the distinct PDT efficacies of ZnPc1 and ZnPc2 arise from their structural and photophysical differences, ROS generation efficiency, and cell-specific responses. The greater Q-band intensity of ZnPc1, further support its enhanced ability to electronic transition, absorb light and generate ROS efficiently. Conversely, ZnPc2, while still effective, requires higher concentrations to achieve significant cytotoxicity, likely due to its lower ROS generation capacity. These findings underscore the critical role of structural modifications in tuning phthalocyanine-based photosensitizers to optimize PDT outcomes in different cancer cell types.

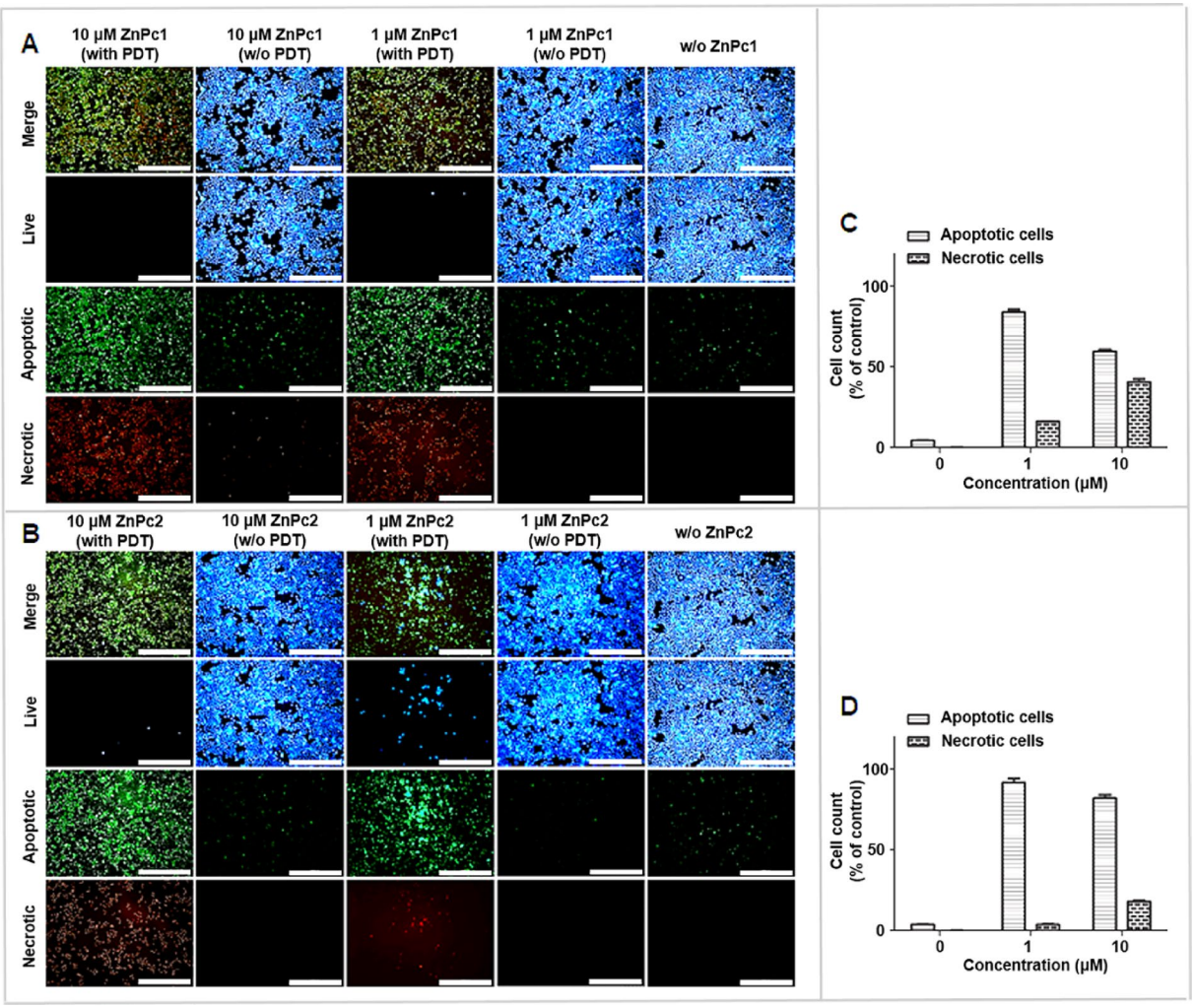

Fig. 9. PDT-induced cellular death mechanism on FaDu cells mediated by (**A**, **C**) ZnPc1 and (**B**, **D**) ZnPc2 molecules. Apoptotic cells (Apoxin Green dye, green), living cells (Cyto Calcein Violet 450, blue) and necrotic cells (7-AAD, red). Scale bar: 200 μm.

PDT utilizing Pc molecules in monolayer cultures of cancer cells results in significant cell death, predominantly through apoptosis. This is demonstrated by the significant phototoxicity observed upon exposure to light. These findings are consistent with prior research suggesting that ZnPc can efficiently trigger cell death by producing ROS and activating apoptotic pathways[37]. Nevertheless, because of the excessively simplistic characteristics of these cultures, the findings cannot be directly applied in clinical settings. 3D spheroids, in contrast to 2D monolayer cultures, provide a more precise depiction of physiological circumstances by simulating cell–cell interactions within the tumor. This serves as a valuable intermediary between 2D cell cultures and in vivo studies and provides an understanding of its potential clinical efficacy[55]. However, the penetration of photosensitizers and distribution of phototoxic effects are less uniform in spheroids. The varied response to PDT in spheroids is caused by the dense extracellular matrix and restricted transport of oxygen and therapeutics into the core[56].

The use of spheroids, which more closely represent the 3D structure of tumors, highlighted the capacity of Pc molecules to efficiently destroy cancer cells within a complex tissue architecture. Although spheroids present challenges, including restricted drug penetration and hypoxic conditions, Pc molecules exhibited significant PDT activity, indicating that these molecules have the ability to penetrate and induce cytotoxicity even within more complex systems. In contrast, the PDT activities of ZnPcs were lower in the cancer spheroids than in the monolayer cells, with a higher distribution of living cells observed in the spheroid cores. Reduced PDT activity in spheroids has also been reported in various cancer[57,58]. The mechanism of PDT is dependent on molecular oxygen, and unlike monolayer cells, the presence of a decreasing oxygen gradient towards the core of the spheroids contributes to the decreased activity of PDT. These oxygen gradients and hypoxic conditions as a crucial aspect of cancer, are particularly critical when evaluating the effectiveness of PDT. Therefore, the use of spheroids provides a more reliable prediction of in vivo drug efficacy.

The formation of ROS as a result of the interaction of the photosensitizer with light irreversibly oxidizes critical cellular components, leading to tissue damage, which underpins the fundamental mechanism of PDT. Numerous studies have elucidated the critical role of molecular oxygen in PDT, in which cellular damage is

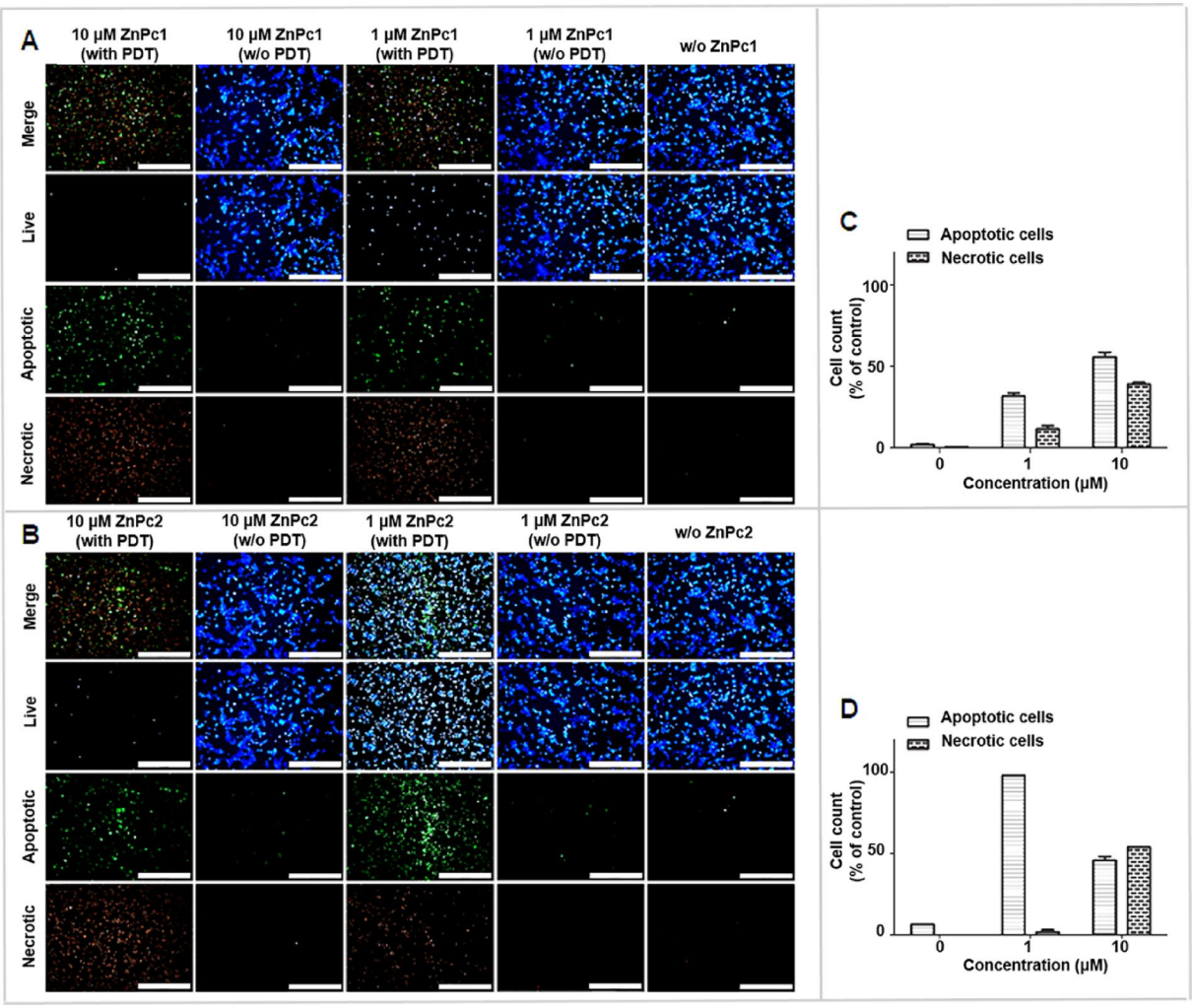

Fig. 10. PDT-induced cellular death mechanism on A253 cells mediated by (**A**, **C**) ZnPc1 and (**B**, **D**) ZnPc2 molecules. Apoptotic cells (Apoxin Green dye, green), living cells (Cyto Calcein Violet 450, blue) and necrotic cells (7-AAD, red). Scale bar: 200 μm.

primarily caused by ROS formed as a result of energy transfer from Pc molecules to nearby molecular oxygen[59,60]. The results highlighted the critical role of ROS in the cytotoxic response, as evidenced by the correlation between levels of ROS production and the degree of cytotoxicity, indicating that the PDT-induced cytotoxicity of the molecules was predominantly reliant on ROS production. Delayed ROS production induced by both molecules was significantly higher than the immediate ROS levels. This demonstrated that both molecules were more effective in initiating ROS production over a longer period than immediately after PDT, indicating a sustained oxidative stress response in the cells. The delayed increase in ROS levels observed 24 h post-PDT, despite no significant increase at 30 min, suggests a secondary oxidative stress rather than immediate photochemical ROS generation. This phenomenon may be attributed to mitochondrial dysfunction, wherein PDT-induced damage disrupts mitochondrial membrane potential, leading to a progressive leakage of ROS over time[61]. Moreover, the activation of apoptotic and necrotic pathways induced by PDT can lead to sustained ROS generation as cellular death processes progress[62]. Another contributing factor could be endoplasmic reticulum (ER) stress, which induces unfolded protein responses and intracellular calcium fluctuations, further exacerbating oxidative stress at later time points[63]. Furthermore, the impairment of autophagy may contribute to the delayed accumulation of ROS. Although autophagy initially serves as a protective mechanism against oxidative stress, its dysfunction over time can result in prolonged ROS generation and the progression of apoptosis[64]. Mitochondrial iron metabolism dysregulation following PDT may also contribute to the prolonged accumulation of ROS, as mitochondrial iron homeostasis is essential for oxidative stress regulation[65]. Morover, the intracellular distribution and activation kinetics of the photosensitizer may influence ROS dynamics, particularly if its metabolic activation occurs gradually[66]. Collectively, these mechanisms indicate that the late-phase ROS increase can be a consequence of sustained cellular stress, mitochondrial impairment, and apoptotic progression rather than direct photodynamic action alone. To understand this mechanistic framework, comprehensive kinetic studies are essential for elucidating the temporal dynamics of ROS generation and its underlying regulatory mechanisms.

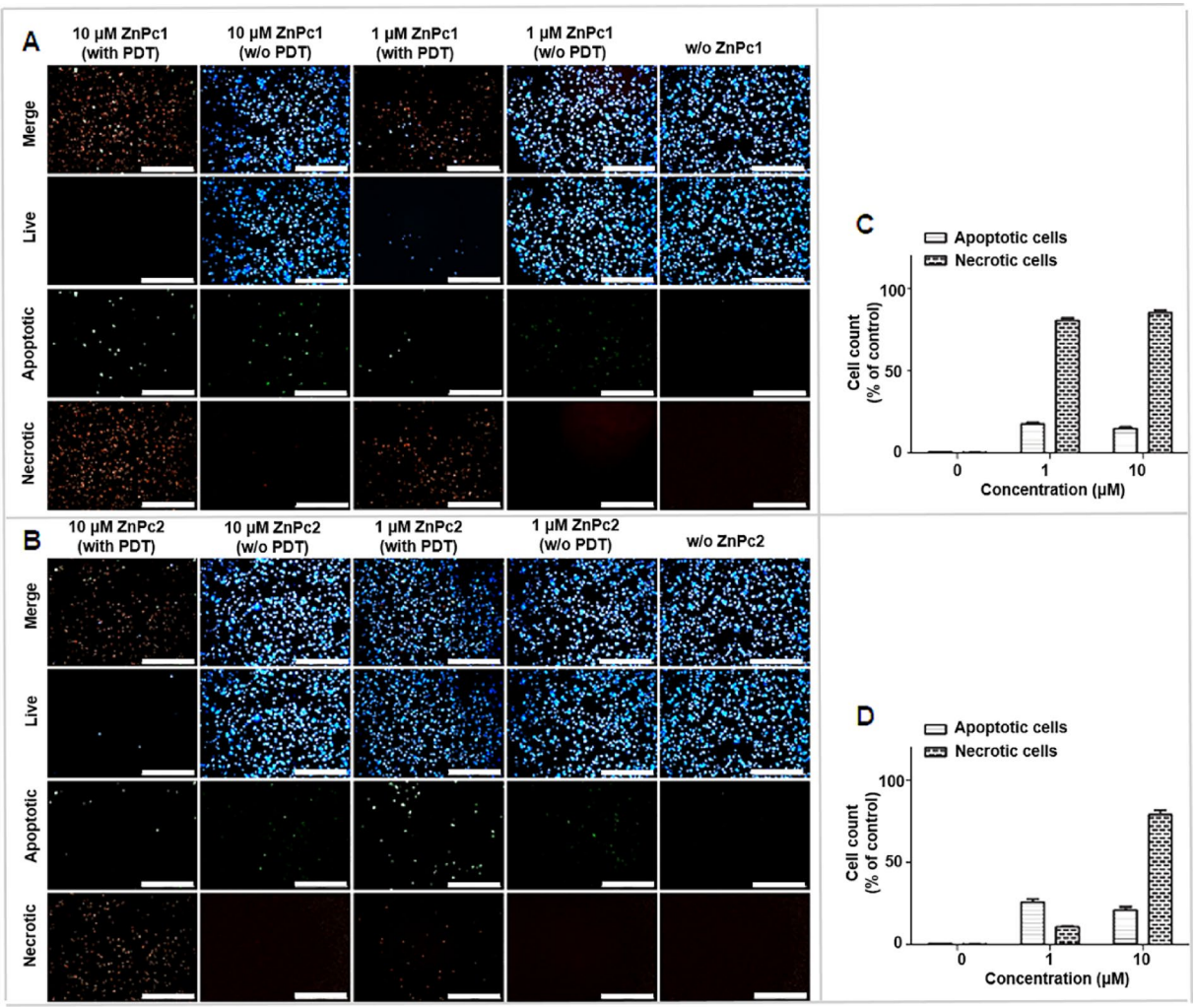

Fig. 11. PDT-induced cellular death mechanism on HT29 cells mediated by (**A**, **C**) ZnPc1 and (**B**, **D**) ZnPc2 molecules. Apoptotic cells (Apoxin Green dye, green), living cells (Cyto Calcein Violet 450, blue) and necrotic cells (7-AAD, red). Scale bar: 200 μm.

PDT-induced ROS production triggers cellular damage in the form of apoptosis, necrosis, or a combination of both. The efficacy of ZnPcs in inducing cell death through both apoptosis and necrosis has been highlighted in numerous studies, which reported that PDT with ZnPcs predominantly induced apoptosis through ROS production and activation of mitochondrial pathways[67–69]. Furthermore, Valli et al. (2020) demonstrated that ZnPc-mediated PDT triggered cell death through both apoptosis and autophagy, indicating a complex interplay of cell death mechanisms dependent on cellular context and ZnPc concentration[70]. These results suggest that Pc-mediated PDT induces different cellular death mechanisms that are primarily affected by the cell type, concentration, and chemical structure of the photosensitizer.

These findings highlight the potential of these molecules as promising candidates for PDT, with ZnPc1 demonstrating superior efficacy as a photosensitizer for therapeutic applications.

Conclusion

In this study, peripheral and non-peripheral tetra-substituted cationic zinc phthalocyanines (ZnPc1 and ZnPc2) were synthesized and characterized. The overall results demonstrated the promising potential of zinc phthalocyanines (ZnPc1 and ZnPc2) as photosensitizers in PDT against different cancer cells using both monolayer culture and 3D spheroid models. Both molecules exhibited negligible cytotoxicity in the dark, meeting the crucial requirements for effective PDT agents. Upon light activation, they induced significant cytotoxicity, particularly in FaDu cells, which indicated their efficacy. Both cytotoxicity and real-time proliferation inhibition assays confirmed the potency of the molecules, particularly ZnPc1, with lower IC50 values in all cell lines. The 3D spheroid model, which provided a more accurate representation of in vivo tumors, validated the effectiveness of ZnPc1, confirming its non-toxic nature in the dark and significant cytotoxicity upon light activation. Their ability to penetrate and effectively induce cytotoxicity in 3D spheroids suggests that ZnPc could be a valuable photosensitizer for PDT, capable of overcoming the challenges posed by the complex 3D architecture of

tumors. ZnPc1-mediated PDT induced higher immediate and delayed ROS production across all cell lines, correlating with the cytotoxicity results and highlighting the role of ROS in the efficacy of PDT. The study also demonstrated differences in the cellular death mechanisms induced by PDT, with apoptosis as the primary cell death mechanism at low doses and increased necrosis at higher doses. In photochemical measurements, it was observed that ZnPc1 and ZnPc2 can produce singlet oxygen in both solvents (0.79 for ZnPc1 and 0.60 for ZnPc2 in DMSO; 0.47 for ZnPc1 and 0.37 for Znpc2 in aqua solutions). The results clearly demonstrate that peripheral substitution significantly enhances singlet oxygen generation, with ZnPc1 consistently outperforming ZnPc2 in both organic and aqueous media. Despite the inability to perform measurements in biological solvents due to the lack of a suitable standard, the superior singlet oxygen yields of ZnPc1 underscore its potential in photodynamic applications. The photochemical results align well with cellular PDT outcomes, reinforcing the conclusion that peripheral substitution in ZnPc1 contributes to its superior photodynamic performance. These findings reveal the potential of Pc molecules, particularly ZnPc1, for cancer therapy, especially in head and neck squamous cell carcinoma. Future studies should focus on optimizing ZnPc delivery and understanding its mechanism of action in more complex tumor models to further enhance its clinical applicability.

Data availability

The data supporting the findings of this study are available from the corresponding author upon reasonable request.

Received: 27 December 2024; Accepted: 30 June 2025
Published online: 11 July 2025

References

1. Hanahan, D. Hallmarks of cancer: New dimensions. *Cancer Discov.* **12**, 31–46 (2022).
2. Allamyradov, Y. et al. Photodynamic therapy review: Past, present, future. Opportunities and challenges. *Photochem* **4**, 434–461 (2024).
3. Brown, S. B., Brown, E. A. & Walker, I. The present and future role of photodynamic therapy in cancer treatment. *Lancet Oncol.* **5**, 497–508 (2004).
4. Dougherty, T. J. et al. Photodynamic therapy. *J. Natl. Cancer Inst.* **90**, 889–905 (1998).
5. Plaetzer, K., Kiesslich, T., Verwanger, T. & Krammer, B. The modes of cell death induced by PDT: An overview. *Med. Laser Appl* **18**, 7–19 (2003).
6. Kwiatkowski, S. et al. Photodynamic therapy—mechanisms, photosensitizers and combinations. *Biomed. Pharmacother.* **106**, 1098–1107 (2018).
7. Chilakamarthi, U. & Giribabu, L. Photodynamic therapy: Past, present and future. *Chem. Rec.* **17**, 775–802 (2017).
8. Plaetzer, K., Krammer, B., Berlanda, J., Berr, F. & Kiesslich, T. Photophysics and photochemistry of photodynamic therapy: Fundamental aspects. *Lasers Med. Sci.* **24**, 259–268 (2009).
9. Baptista, M. S. et al. Type I and type II photosensitized oxidation reactions: guidelines and mechanistic pathways. *Photochem. Photobiol.* **93**, 912–919 (2017).
10. Abrahamse, H. & Hamblin, M. R. New photosensitizers for photodynamic therapy. *Biochem. J.* **473**, 347–364 (2016).
11. DeRosa, M. C. & Crutchley, R. J. Photosensitized singlet oxygen and its applications. *Coord. Chem. Rev.* **233**, 351–371 (2002).
12. Henderson, B. W. & Dougherty, T. J. How does photodynamic therapy work?. *Photochem. Photobiol.* **55**, 145–157 (1992).
13. Dlugaszewska, J. et al. Antimicrobial and anticancer photodynamic activity of a phthalocyanine photosensitizer with *N*-methyl morpholiniumethoxy substituents in non-peripheral positions. *J. Inorg. Biochem.* **172**, 67–79 (2017).
14. Plaetzer, K., Kiesslich, T., Krammer, B. & Hammerl, P. Characterization of the cell death modes and the associated changes in cellular energy supply in response to AlPcS4-PDT. *Photochem. Photobiol. Sci.* **1**, 172–177 (2002).
15. Agostinis, P. et al. Photodynamic therapy of cancer: An update. *CA: A Cancer J. Clin.* **61**, 250–281 (2011).
16. Roguin, L. P., Chiarante, N., Vior, M. C. G. & Marino, J. Zinc(II) phthalocyanines as photosensitizers for antitumor photodynamic therapy. *Int. J. Biochem. Cell Biol.* **114**, 105575 (2019).
17. Li, X. et al. Phthalocyanines as medicinal photosensitizers: Developments in the last five years. *Coord. Chem. Rev.* **379**, 147–160 (2019).
18. Hamam, K. J. & Alomari, M. I. A study of the optical band gap of zinc phthalocyanine nanoparticles using UV–Vis spectroscopy and DFT function. *Appl. Nanosci.* **7**, 261–268 (2017).
19. Kessel, D. Correlation between subcellular localization and photodynamic efficacy. *J. Porphyr. Phthalocyanines* **8**, 1009–1014 (2004).
20. Ishii, K. Functional singlet oxygen generators based on phthalocyanines. *Coord. Chem. Rev.* **256**, 1556–1568 (2012).
21. Rosenthal, I. Phthalocyanines as photodynamic sensitizers. *Photochem. Photobiol.* **53**, 859–870 (1991).
22. Li, X., Lee, D., Huang, J. D. & Yoon, J. Phthalocyanine-assembled nanodots as photosensitizers for highly efficient type I photoreactions in photodynamic therapy. *Angew. Chem.* **130**, 10033–10038 (2018).
23. Dumoulin, F., Durmuş, M., Ahsen, V. & Nyokong, T. Synthetic pathways to water-soluble phthalocyanines and close analogs. *Coord. Chem. Rev.* **254**, 2792–2847 (2010).
24. Özçeşmeci, M., Ecevit, Ö. B., Sürgün, S. & Hamuryudan, E. Tetracationic fluorinated zinc(ii) phthalocyanine: Synthesis, characterization and DNA-binding properties. *Dyes Pigm.* **96**, 52–58 (2013).
25. Koçan, H. et al. Photophysicochemical, calf thymus DNA binding and in vitro photocytotoxicity properties of tetra-morpholinoethoxy-substituted phthalocyanines and their water-soluble quaternized derivatives. *J. Biol. Inorg. Chem.* **22**, 1251–1266 (2017).
26. Özçeşmeci, M., Baş, S. S., Akkurt, B., Bolkent, Ş & Hamuryudan, E. Synthesis, characterization and staining performance of peripherally and non-peripherally substituted metallo-phthalocyanines bearing 1, 3-bis-(trimethylamino)-2-propoxy groups. *New J. Chem.* **44**, 7786–7794 (2020).
27. Özçeşmeci, M., Sancar-Baş, S., Akkurt, B., Hamuryudan, E. & Bolkent, Ş. Synthesis and biological uses of A3B type water-soluble phthalocyanine alternate to alcian blue. *ChemistrySelect* **3**, 12805–12812 (2018).
28. Ajmal, A. et al. Photocatalytic degradation of textile dyes on Cu_2O-CuO/TiO_2 anatase powders. *J. Environ. Chem. Eng.* **4**, 2138–2146 (2016).
29. Akçay, H. T., Bayrak, R., Karslioğlu, S. & Şahin, E. Synthesis, characterization and spectroscopic studies of novel peripherally tetra-imidazole substituted phthalocyanine and its metal complexes, the computational and experimental studies of the novel phthalonitrile derivative. *J. Organomet. Chem.* **713**, 1–10 (2012).
30. Gunaydin, G., Gedik, M. E. & Ayan, S. Photodynamic therapy—current limitations and novel approaches. *Front. Chem.* **9**, 691697 (2021).

31. Li, M. et al. Photodynamic antimicrobial chemotherapy with cationic phthalocyanines against Escherichia coli planktonic and biofilm cultures. *RSC Adv.* **7**, 40734–40744 (2017).
32. Soriano, J., Villanueva, A., Stockert, J. C. & Cañete, M. Regulated necrosis in HeLa cells induced by ZnPc photodynamic treatment: A new nuclear morphology. *Int. J. Mol. Sci.* **15**, 22772–22785 (2014).
33. Alvarez, N. & Sevilla, A. Current advances in photodynamic therapy (PDT) and the future potential of PDT-combinatorial cancer therapies. *Int. J. Mol. Sci.* **25**, 1023 (2024).
34. Kocaağa, N., Türkkol, A., Bilgin, M. D. & Erdoğmuş, A. The synthesis of novel water-soluble zinc(II) phthalocyanine based photosensitizers and exploring of photodynamic therapy activities on the PC3 cancer cell line. *Photochem. Photobiol. Sci.* **22**, 2037–2053 (2023).
35. Ahmetali, E. et al. Photodynamic therapy activities of phthalocyanine-based macromolecular photosensitizers on MCF-7 breast cancer cells. *J. Macromol. Sci. Part A* **58**, 748–757 (2021).
36. Kuzyniak, W. et al. Novel zinc phthalocyanine as a promising photosensitizer for photodynamic treatment of esophageal cancer. *Int. J. Oncol.* **50**, 953–963 (2017).
37. Manoto, S. L., Houreld, N., Hodgkinson, N. & Abrahamse, H. Modes of cell death induced by photodynamic therapy using zinc phthalocyanine in lung cancer cells grown as a monolayer and three-dimensional multicellular spheroids. *Molecules* **22**, 791 (2017).
38. Schmidt, J. et al. Novel zinc-and silicon-phthalocyanines as photosensitizers for photodynamic therapy of cholangiocarcinoma. *Int. J. Mol. Med.* **42**, 534–546 (2018).
39. Kolarova, H., Tomankova, K., Bajgar, R., Kolar, P. & Kubinek, R. Photodynamic and sonodynamic treatment by phthalocyanine on cancer cell lines. *Ultrasound Med. Biol.* **35**, 1397–1404 (2009).
40. Kocaağa, N., Türkkol, A., Bilgin, M. D. & Erdoğmuş, A. Synthesis and characterization of indium(III) phthalocyanines with different Schiff Base groups for application in photodynamic therapy. *J. Photochem. Photobiol. A* **466**, 116373 (2025).
41. Isik, S. et al. Anti-angiogenic effects of cationic zinc(II) phthalocyanine derivatives through photodynamic therapy. *Sci. Rep.* **15**, 2498 (2025).
42. Akkoç, B. et al. Pegylated metal-free and zinc(II) phthalocyanines: synthesis, photophysicochemical properties and in vitro photodynamic activities against head, neck and colon cancer cell lines. *Dalton Trans.* **51**, 10136–10147 (2022).
43. Gomes, M. T. et al. Phosphatidylserine externalization by apoptotic cells is dispensable for specific recognition leading to innate apoptotic immune responses. *J. Biol. Chem.* **298**, 102034 (2022).
44. Vummidi, B. R., Noreen, F., Alzeer, J., Moelling, K. & Luedtke, N. W. Photodynamic agents with anti-metastatic activities. *ACS Chem. Biol.* **8**, 1737–1746 (2013).
45. Marino, J., Vior, M. C. G., Dicelio, L. E., Roguin, L. P. & Awruch, J. Photodynamic effects of isosteric water-soluble phthalocyanines on human nasopharynx KB carcinoma cells. *Eur. J. Med. Chem.* **45**, 4129–4139 (2010).
46. Wöhrle, D. et al. Synthesis of positively charged phthalocyanines and their activity in the photodynamic therapy of cancer cells. *Photochem. Photobiol.* **51**, 351–356 (1990).
47. Nyokong, T. Effects of substituents on the photochemical and photophysical properties of main group metal phthalocyanines. *Coord. Chem. Rev.* **251**, 1707–1722 (2007).
48. Celep, K. et al. Exploring improved strategies for therapeutic studies and biological activities of novel zinc and indium phthalocyanines. *Dalton Trans.* **53**, 17381–17393 (2024).
49. Özten, Ö. et al. Potential zinc phthalocyanine-based photosensitizer for photodynamic therapy: Photophysical, theoretical and in vitro studies. *J. Inorg. Biochem.* **270**, 112958 (2025).
50. Granados-Tavera, K. et al. Synergistic effect of ultrasound and light to efficient singlet oxygen formation for photodynamic purposes. *Dyes Pigm.* **210**, 110986 (2023).
51. Turkkol, A. et al. Hybrid sono-photodynamic combination therapy mediated by water-soluble gallium phthalocyanine enhances the cytotoxic effect against breast cancer cell lines. *ACS Appl. Bio Mater.* **7**, 2725–2733 (2024).
52. Koca, B. et al. Exploring the photophysics of polyfluorinated phthalocyanine derivatives as potential theranostic agents. *J. Phys. Chem. C* **123**, 24417–24425 (2019).
53. Erdoğmuş, A. & Nyokong, T. New soluble methylendioxy-phenoxy-substituted zinc phthalocyanine derivatives: Synthesis, photophysical and photochemical studies. *Polyhedron* **28**, 2855–2862 (2009).
54. Erdoğmuş, A. & Nyokong, T. Synthesis of zinc phthalocyanine derivatives with improved photophysicochemical properties in aqueous media. *J. Mol. Struct.* **977**, 26–38 (2010).
55. Allen, C. M., Sharman, W. M. & Van Lier, J. E. Current status of phthalocyanines in the photodynamic therapy of cancer. *J. Porphyr. Phthalocyanines* **5**, 161–169 (2001).
56. Evans, C. L. Three-dimensional in vitro cancer spheroid models for photodynamic therapy: Strengths and opportunities. *Front. Phys.* **3**, 15 (2015).
57. Simelane, N. W. N. & Abrahamse, H. Zinc phthalocyanine loaded-antibody functionalized nanoparticles enhance photodynamic therapy in monolayer (2-D) and multicellular tumour spheroid (3-D) cell cultures. *Front. Mol. Biosci.* **10**, 1340212 (2024).
58. Chiarante, N., Vior, M. C. G., Awruch, J., Marino, J. & Roguin, L. P. Phototoxic action of a zinc(II) phthalocyanine encapsulated into poloxamine polymeric micelles in 2D and 3D colon carcinoma cell cultures. *J. Photochem. Photobiol. B* **170**, 140–151 (2017).
59. Benov, L. Photodynamic therapy: Current status and future directions. *Med. Princ. Pract.* **24**, 14–28 (2015).
60. Zhang, Z.-J., Wang, K.-P., Mo, J.-G., Xiong, L. & Wen, Y. Photodynamic therapy regulates fate of cancer stem cells through reactive oxygen species. *World J. Stem Cells* **12**, 562 (2020).
61. Gomes, Rd. Á. N. et al. Mitochondrial dysfunction mediates neuronal cell response to DMMB photodynamic therapy. *Biochim. Biophys. Acta (BBA)-Mol. Cell Res.* **1870**, 119429 (2023).
62. Chen, Y. et al. Apoptosis induced by methylene-blue-mediated photodynamic therapy in melanomas and the involvement of mitochondrial dysfunction revealed by proteomics. *Cancer Sci.* **99**, 2019–2027 (2008).
63. Moserova, I. & Kralova, J. Role of ER stress response in photodynamic therapy: ROS generated in different subcellular compartments trigger diverse cell death pathways. *PLoS ONE* **7**, e32972 (2012).
64. He, C., Xia, J., Gao, Y., Chen, Z. & Wan, X. Chlorin A-mediated photodynamic therapy induced apoptosis in human cholangiocarcinoma cells via impaired autophagy flux. *Am. J. Transl. Res.* **12**, 5080 (2020).
65. Hung, H.-I., Schwartz, J. M., Maldonado, E. N., Lemasters, J. J. & Nieminen, A.-L. Mitoferrin-2-dependent mitochondrial iron uptake sensitizes human head and neck squamous carcinoma cells to photodynamic therapy. *J. Biol. Chem.* **288**, 677–686 (2013).
66. Dewaele, M. et al. Autophagy pathways activated in response to PDT contribute to cell resistance against ROS damage. *J. Cell Mol. Med.* **15**, 1402–1414 (2011).
67. Barut, B. et al. Evaluation of photodynamic therapy effects of novel zinc(II) phthalocyanine through a possible interaction with toll-like receptor signaling pathway. *Appl. Organomet. Chem.* **37**, e7039 (2023).
68. Ogbodu, R. O. et al. Photodynamic therapy of hepatocellular carcinoma using tetra-triethyleneoxysulfonyl zinc phthalocyanine as photosensitizer. *J. Photochem. Photobiol. B* **208**, 111915 (2020).
69. Ma, C. et al. Caspase-1 regulates the apoptosis and pyroptosis induced by phthalocyanine zinc-mediated photodynamic therapy in breast cancer MCF-7 cells. *Molecules* **28**, 5934 (2023).
70. Valli, F., Vior, M. C. G., Roguin, L. P. & Marino, J. Crosstalk between oxidative stress-induced apoptotic and autophagic signaling pathways in Zn(II) phthalocyanine photodynamic therapy of melanoma. *Free Radic. Biol. Med.* **152**, 743–754 (2020).

Acknowledgements
"This study was supported by the Scientific and Technological Research Council of Turkey (TUBITAK) under Grant Number 216S387. The authors thank TUBITAK for their support."

Author contributions
S.I. and M.S. designed the concept and cellular based experiments and analyzed the data. S.I. performed the experiments. A.E performed photochemical properties. E.H., M.O., and A.K.B. synthesized and characterized the Pc molecules. M.S. and O.C. supervised the study. S.I. drafted the manuscript. The manuscript was written with the contributions of all authors. All authors approved the final version of the manuscript.

Declarations

Competing interests
The authors declare no competing interests.

Additional information
Supplementary Information The online version contains supplementary material available at https://doi.org/10.1038/s41598-025-09630-7.

Correspondence and requests for materials should be addressed to O.C. or M.S.

Reprints and permissions information is available at www.nature.com/reprints.

Publisher's note Springer Nature remains neutral with regard to jurisdictional claims in published maps and institutional affiliations.